Generation of a Novel High-Affinity Antibody Binding to PCSK9 Catalytic Domain with Slow Dissociation Rate by CDR-Grafting, Alanine Scanning and Saturated Site-Directed Mutagenesis

Zhengli Bai
China Pharmaceutical University
Menglong Xu
China Pharmaceutical University
Ying Mei
China Pharmaceutical University
Tuo Hu
China Pharmaceutical University
Panpan Zhang
China Pharmaceutical University
Manman Chen
China Pharmaceutical University
Wenxiu Lv
China Pharmaceutical University
Chenchen Lu
China Pharmaceutical University
Shuhua Tan (tanshuhua163@163.com)
China Pharmaceutical University https://orcid.org/0000-0002-4992-8876

Original article

Keywords: single-chain variable fragment (scFv), Escherichia coli (E. coli), Alanine scanning, saturated site-directed mutagenesis, PCSK9, Molecular docking

Posted Date: October 21st, 2021

DOI: https://doi.org/10.21203/rs.3.rs-957578/v1

Abstract

Inhibition of Proprotein convertase subtilisin/kexin type 9 (PCSK9) has become an attractive therapeutic strategy for lowering low-density lipoprotein cholesterol (LDL-C). In this study, a novel high affinity humanized IgG1 mAb (named h5E12-L230G) targeting the catalytic domain of human PCSK9 (hPCSK9) was generated by using CDR-grafting, alanine-scanning mutagenesis, and saturated site-directed mutagenesis. To eliminate the cytotoxic effector functions and mitigate the heterogeneity, the heavy-chain constant region of h5E12-L230G was modified with L234A/L235A/N297G mutations and C-terminal lysine deletion. The biolayer interferometry (BLI) binding assay and molecular docking study revealed that h5E12-L230G binds to the catalytic domain of hPCSK9 with nanomolar affinity (K_D =1.72 nM) and an extremely slow dissociation rate (k_{off}, 4.84×10^{-5} s^{-1}), which interprets its quite low binding energy (-54.97 kcal/mol) with hPCSK9. Additionally, h5E12-L230G elevated the levels of LDLR and enhanced the LDL-C uptake in HepG2 cells, as well as reduced the serum LDL-C and total cholesterol (TC) levels in hyperlipidemic mouse model with high potency comparable to Alirocumab. Our data suggest that h5E12-L230G is a highly potent antibody binding to PCSK9 catalytic domain with slow dissociation rate which may be utilized as a therapeutic candidate for treating hypercholesterolemia and relevant cardiovascular diseases.

Introduction

Hypercholesterolemia with elevated plasma low-density lipoprotein cholesterol (LDL-C) levels is a major risk factor for the development of cardiovascular diseases (CVDs) (Rader et al. 2008, Tietge 2014). Accumulating experimental and clinical studies implicate that the level of LDL-C is positively proportional to the incidence of CVDs (Mihaylova et al. 2012, Silverman et al. 2016, Egom et al. 2019). Plasma LDL-C is cleared through its uptake into cells upon binding the low-density lipoprotein receptor (LDLR) on the surface of hepatocytes, then the LDL-C/LDL-R complex is sent to lysosome for LDL-C degradation, and the released LDLR is recirculated to the cell surface (Brown et al. 1986).

Proprotein convertase subtilisin/kexin type 9 (PCSK9), a member of the subtilisin serine protease family, has been demonstrated to be able to raise LDL-C level through binding to epidermal growth factor(A) and β-propeller domains of LDLR by its catalytic domain and prodomain (Cunningham et al. 2007, Holla et al. 2007, Nassoury et al. 2007, Poirier et al. 2009). In human, mechanistic studies of PCSK9 have shown that gain-of-function mutations cause a form of familial hypercholesterolemia, whereas loss-of-function mutations result in significantly decreased LDL-C level and cardiovascular risk (Abifadel et al. 2003, Timms et al. 2004, Cohen et al. 2006, Wu et al. 2014). Several different approaches have been explored as means to inhibit or reduce PCSK9, including antisense oligonucleotides (van Poelgeest et al. 2015), lipidoid nanoparticle (LNP) formulated short interfering RNA (siRNAs) directed against the PCSK9 messenger RNA (mRNA) (Lindholm et al. 2012), antibodies directed against circulating PCSK9 protein (Schwartz et al. 2014, Stroes et al. 2014, Yokote et al. 2017) and small peptides that blocked the PCSK9/LDLR interaction (Mitchell et al. 2014). Taken together, these findings indicate that PCSK9 represents an excellent target for curing hypercholesterolemia as well as other relevant diseases (Farnier 2018, Schmit et al. 2019). Monoclonal antibodies (mAbs), because of their high specificity toward a given target, represent a unique class of novel therapeutics as PCSK9 inhibitors.

Hybridoma technique, invented by Köhler and Milstein, is a well-established robust method for generating mAbs targeting the antigen of interest (KÖHler et al. 1975, Li et al. 2019, Luo et al. 2020, Ren et al. 2021). Hybridoma

technology can screen hybridoma cell lines which not only have the immortality of myeloma cells but also have the ability of splenocytes to secrete antibodies by fusing myeloma cells with splenocytes from immunized mice (Elgundi et al. 2017). However, murine mAbs prepared by the hybridoma technique may induce the human anti-mouse antibodies (HAMA) response which limits its utility and efficacy in clinical treatment (Chan et al. 2001).

Humanization of murine mAbs is crucial to circumvent the problem. The first humanization strategy is to construct chimeric antibodies by substituting the murine constant region with an appropriate human constant region to reduce the content of heterologous sequences (Morrison et al. 1984). Several chimeric antibodies have been approved by FDA, including ramucirumab, brentuximab, dinutuximab, etc. The variable domains of chimeric antibodies that consist of framework regions (FRs) and complementarity determining regions (CDRs) are completely murine, while FRs are not necessarily required for antigen recognition (Chiu et al. 2016). Based on it, grafting murine CDRs onto human germline FRs and retaining the residues in murine FRs which may play a key role in maintaining the conformational integrity of CDRs to construct a CDR-grafted antibody can further reduce the immunogenicity (Haidar et al. 2012, Safdari et al. 2013). Humanization and affinity maturation are the most frequently applied processes to develop a therapeutic antibody with high affinity to a specific epitope (Inoue et al. 2013, Ko et al. 2015). *In vitro* affinity maturation of mAbs mimics the process of *in vivo* affinity maturation which relies on somatic hypermutation of immunoglobulin genes and positive clonal selection (Ersching et al. 2017). The most commonly used *in vitro* affinity maturation technologies are (1) site-directed mutagenesis and random mutagenesis consisting in the introduction of mutagenesis specifically or randomly throughout the gene, (2) chain shuffling that recombines the heavy and light chains of different antibodies with high affinity, (3) phage display which allows screening the desired antibody from a large library with millions to trillions of variants (Levin et al. 2006, Sheedy et al. 2007, Yun et al. 2019).

In this work, we describe the generation, humanization and *in vitro* affinity maturation of a hybridoma-derived anti-PCSK9 antibody by using CDR-grafting, alanine-scanning mutagenesis, and saturated site-directed mutagenesis methods. Humanization and affinity maturation of the generated murine antibody was conducted using the single-chain variable fragment (scFv) format for the reason that scFvs are much more convenient to modify and produce in *E. coli* host, then the selected optimized scFvs were reformatted into full-length IgG and expressed transiently in CHO-3E7 mammalian cells for further identification.

Material And Methods

Materials

MEM, DMEM, Opti-MEM, and Pluronic-F68 were purchased from Thermo Fisher Scientific (Waltham, MA, USA). Fetal bovine serum (FBS), penicillin G sodium salt, streptomycin solution, and hypoxanthine-aminopterin-thymidine (HAT) were obtained from MilliporeSigma (Burlington, MA, USA). HyClone™ HyCell™ CHO Medium was purchased from GE Healthcare (Piscataway, NJ, USA). 25 kDa Linear polyethyleneimine (LPEI) was obtained from Polysciences (Warrington, Pennsylvania, USA). Quickantibody-Mouse 5W adjuvant (Cat# KX0210041) was obtained from Biodragon Immunotechnologies (Beijing, China). Bovine serum albumin (BSA) was obtained from Biofroxx (Einhausen, Hessen, Germany). Agarose Gel DNA Extraction Kit, RNAiso Plus, and PrimeScript RT Reagent Kit with gDNA Eraser were bought from TaKaRa (Dalian, Liaoning, China). Rabbit anti-PCSK9 antibody (Cat# ab181142) and rabbit anti-LDLR antibody (Cat# ab52818) were obtained from Abcam (Cambridge, UK). Glutamine, TMB substrate, IPTG, rabbit anti-GAPDH antibody (Cat# D110016), HRP-conjugated goat anti-rabbit

IgG (Cat# D110058), and Alexa Fluor 488®-conjugated goat anti-rabbit IgG (Cat# D110061) were bought from BBI (Toronto, ON, Canada). LDL labeled with 1, 1'-dioctadecyl - 3, 3, 3', 3'-tetramethyl-indocarbocyanine perchlorate (DiI-LDL) was obtained from Yiyuan Biotechnologies (Guangzhou, Guangdong, China). Commercial test kits for LDL-C, TC, TG, and HDL-C were obtained from Nanjing Jiancheng Bioengineering Institute (Nanjing, Jiangsu, China).

Bacterial strains and cell lines

Escherichia coli (*E. coli*) strains DH5α and BL21 (DE3) were used as hosts for plasmid preparation and single-chain variable fragment (scFv) prokaryotic expression, respectively. Chinese hamster ovary (CHO-3E7) cells were obtained from Genscript Biotech (Nanjing, China), cultured in HyClone™ HyCell™ CHO Medium, and used as hosts for IgG1 eukaryotic transient-expression. Mouse myeloma cell line SP2/0 was purchased from American Type Culture Collection (ATCC, Manassas, VA, USA) and cultured in DMEM medium supplemented with penicillin (100 U/ml), streptomycin (100 μg/ml) and 10% (v/v) FBS. Human hepatic HepG2 cells were obtained from China Infrastructure of Cell Line Resources (Beijing, China) and maintained at 37°C, 5% CO2, in MEM supplemented with penicillin (100 U/ml), streptomycin (100 μg/ml) and 10% (v/v) FBS. All cells were cultured in a humidified incubator at 37°C in an atmosphere of 5% CO2 in the air.

Antigen preparation

To produce human PCSK9 (hPCSK9) protein, the coding sequence of hPCSK9 (GenBank accession number: NM_174936.3) fused with a Kozak consensus sequence (GCCGCCACC) (Hernández et al. 2019) at the 5'-end and a 6×His-tag gene at the 3'-end was synthesized by GenScript Biotech (Nanjing, China) and subcloned into the eukaryotic expression vector pTT5 using the *Hin*d III and *Eco*R I restriction enzyme sites. The yielded recombinant plasmids were further transiently transfected into suspension CHO-3E7 mammalian cells using PEI transfection reagent as described previously (Stuible et al. 2018). On day 7 post-transfection, the supernatant was purified with a Ni^{2+} Based immobilized metal ion affinity chromatography (Ni-IMAC, GE Healthcare, Piscataway, NJ, USA), followed by Superdex^{TM} 200 HR 10/300GL size-exclusion chromatography (GE Healthcare) according to the manufacturer's instructions. Protein concentration was determined by using the BCA protein assay kit (Biomiga, San Diego, USA).

BALB/c mice immunization

Purified hPCSK9 protein (20 μg per mouse) was emulsified with an equal volume of Quickantibody-Mouse 5W adjuvant and intramuscularly injected into the hind legs of female BALB/c mice (6-8-wk, Qinglongshan Experimental Animal Breeding Farm, Nanjing, China) on day 1 and day 21. The final boost (50 μg of hPCSK9 protein) was given intraperitoneally on day 35 without adjuvant. Three days after the final booster immunization, orbital blood of mice was collected for antibody titer detection. When the antibody titters attained 1:100000, the cell fusion was conducted.

Cell fusion and hybridoma screening

According to standard procedures(KÖHler 1975, Kim et al. 2014), splenocytes were harvested from the immunized mice and fused with SP2/0mouse myeloma cells at a ratio of 5:1 using 50% (w/v) polyethylene glycol (PEG) as a fusion regent, and the resulting hybridomas were then cultured in 96-well plates in hypoxanthine-aminopterin-thymidine (HAT) selective medium supplemented with 20% (w/v) FBS. Afterward, the positive hybridoma cells were screened by indirect ELISA and subcloned three times by limiting dilution method.

The ascites of identified hybridoma were also prepared by injection of 1×10^6 positive hybridoma cells into the peritoneal cavity of pristine-treated BALB/c mice, and the ascites containing specific mAbs were purified by protein A affinity chromatography (Roche, Mannheim, Germany). The isotype of purified mAb was determined using a mouse monoclonal subtype identification kit (KMI-2, ProteinTech Group, Chicago, IL, USA) according to the manufacturer's instruction.

Enzyme-linked immunosorbent assay

The hybridoma cells producing antibodies against hPCSK9 were screened by Enzyme-linked immunosorbent assay (ELISA) using 96-well plates coated with hPCSK9 (1 μg/ml) in coating buffer (0.2 M Na_2CO_3/$NaHCO_3$, pH 9.6) overnight at 4℃. The plates were then blocked with PBS containing 3% (w/v) bovine serum albumin (BSA) for 2 h at 37℃ and incubated with 100 μl of hybridoma supernatants for 2 h at 37℃. Besides, non-competitive phage ELISA with the addition of increasing concentrations of mAb (10^{-1}, 10, 10^2, 10^3, 10^4, 10^5 ng/ml) was also set up to further measure the affinity constant (K_{aff}) of selected mAb as described previously (Beatty et al. 1987). After washing three times with 0.1% Tween in PBS (PBST), HRP-conjugated goat anti-mouse IgG antibody was added and incubated for 1 h at 37℃. Finally, the TMB substrate was added and allowed to develop for 15 minutes at room temperature, and the absorbance at 450 nm was measured using a microplate reader (Thermo Scientific, Waltham, MA, USA).

Western blot analysis

Western blot was performed to detect the protein expression levels of LDLR in HepG2 cells or liver tissues as previously described (Gu et al. 2019). Briefly, the cells or tissues were lysed or homogenized in cold RIPA lysis buffer (Solarbio, Beijing, China) containing 1 mM PMSF on ice for 0.5 h. After centrifugation at 12,000 g for 15 min at 4°C, the cell lysates were collected and total protein concentrations were determined using BCA protein assay. Equal amounts of protein from each sample were subjected to 12% (w/v) SDS-PAGE and transferred to 0.22 μm polyvinylidene fluoride (PVDF) membrane (MerckMillipore, Darmstadt, Germany). After blocking with 0.1% (v/v) TBS-Tween 20 (TBST) containing 5% (w/v) nonfat milk for 2 h at room temperature, the membrane was incubated with corresponding primary antibodies against GAPDH (Cat# D110016, 1:1000) or LDLR (Cat# ab52818, 1:1000) at 4°C overnight, followed by incubation with HRP-conjugated goat anti-rabbit IgG (Cat# D110058, 1:5000) at room temperature for 1 h. Protein bands were detected by enhanced chemiluminescence (ECL) solution (Thermo Scientific, Massachusetts, USA) and quantified by ImageJ software (National Institutes of Health, Bethesda, MD, USA).

LDL-C uptake assay

LDL-C uptake assay was conducted as previously described (Ly et al. 2014, Xu et al. 2020) with slight modification. In brief, HepG2 cells were seeded in black 96-well plates at a density of 3×10^4 cells per well and cultured overnight. Then, cells were pretreated with opti-MEM for 12 h, followed by treatment with 20 μg/ml hPCSK9 protein alone or co-treatment with 50 μg/ml anti-PCSK9 antibodies for 8 h. Thereafter, 20 μg/ml DiI-LDL was added each well and incubated for an additional 4 h. After washing 3 times with PBS in the dark, LDL-C uptake was measured using a multimode microplate reader (Varioskan lux, Thermo scientific) at 520 nm excitation/580 nm emission.

Cloning of V_H and V_L gene from hybridoma cells

Total RNA was isolated from hybridoma cells secreting monoclonal antibody (mAb) against hPCSK9 by RNAiso reagent and quantified by measuring A_{260} nm with Thermo NanoDrop 2000 (Thermo Fisher Scientific). Then the first-strand cDNA was amplified by reverse transcription-polymerase chain reaction (RT-PCR) using PrimeScript™ RT reagent Kit with gDNA Eraser (TaKaRa, Dalian, China) according to the manufacturer's instructions, and the variable region genes of the heavy and light chains of selected mAb were respectively amplified by PCR using PrimeSTAR® HS DNA Polymerase (TaKaRa, Dalian, China) and previously published primer pairs (Wang et al. 2000) with minor modification (Table 1).

Table 1
PCR primers for amplification of V_H and V_L genes

Primer	Sequence (5'-3')
V_H-F	CCGGAATTCSARGTNMAGCTGSAGSAGTC
V_H-R	CCCAAGCTTATAGACAGATGGGGGTGTCGTTTTGGC
V_L-F	CCGGAATTCGAYATTGTGMTSACMCARWCTMCA
V_L-R	CCCAAGCTTGGATACAGTTGGTGCAGCATC

Computer modeling of single-chain variable-fragment antibodies

The three-dimensional (3D) structure models of single-chain variable-fragment antibodies (scFvs) were built via homology modeling using the Schrodinger Suite 2009 (Schrödinger, LLC, New York, NY, USA). Gromacs program, a versatile package in Schrodinger software to perform molecular dynamics, was used to optimize the structure of m5E12scFv in silico and make it closer to the conformation in the natural environment Subsequently, the qualities of the constructed models were evaluated by Ramachandran Plot within Discovery Studio software (Accelrys Software Inc., San Diego, CA, USA). Root mean square deviation (RMSD) is a statistic to assess the deviation degree between resulting and target conformations, which here was used to estimate the model deviation of the constructed models. Thus, the RMSD values of the main chain atoms (C-α, C, N, O) in CDRs between the models were also calculated by Molecular Operating Environment (MOE) software (Chemical Computing Group, Montreal, Canada).

Design of humanized scFvs

Two humanized scFvs were designed based on different antibody humanization methods. The first humanized scFv was designed by transferring murine CDRs onto suitable human consensus FR templates with the highest similarity using a traditional approach called CDR grafting (Verhoeyen et al. 1988). In order to maintain murine CDRs conformation, the key residues, including (a) residues with less than 30% surface accessibility (Pedersen et al. 1994) (b) abnormal residues (Foote et al. 1992), (c) "Vernier" residues located at the FR-CDR junction (De Haard et al. 1999), which may change CDRs conformations were screened by Abcheck (https://www.abcheckantibodies.com/) and Schrodinger Suite 2009. Afterward, another humanized scFv was then designed by back-mutation of these key residues to the amino acids of the original murine mAb.

Construction, expression and purification of scFvs

The genes encoding the humanized scFvs were synthesized at Genscript Biotech and subcloned into the prokaryotic expression vector pET-27b (Novagen, Madison, WI, USA) containing the pectate lyase signal peptide (pelB) of *Erwinia carotovora* (Blanco-Toribio et al. 2015) using primers listed in Table 2. The resulting recombinant plasmids were further transformed into *E. coli* BL21 (DE3) cells through CaCl2 heat shock method, and the transformed *E. coli* BL21 (DE3) cells were cultured in 2×YT medium with 50 μg/ml of kanamycin at 37℃. When the OD_{600} reached 0.6-0.8, the temperature was shifted to 16℃ and 0.2 mM isopropyl-β-galactosidase (IPTG) was added to induce expression for 18 h. The expressed soluble scFvs with C-terminal 6×His-tag were isolated from the periplasm and purified by Ni-NTA affinity chromatography column (GE Healthcare) and Superdex^{TM} 75 HR 10/300GL size-exclusion (GE Healthcare) successively, according to manufactures' protocols.

Table 2
PCR primers for amplification of humanized scFvs

Primer	Sequence (5'-3')
m-F	CATGCCATGGATGAAGTTCAGCTGGAGCAGTCAG
m-R	CCCAAGCTTTCA*ATGGTGATGGTGATGGTG*TTTCAGCTCCAGCTTGGTCC
h-F	CATGCCATGGATCAGGTGCAGCTGGTGCAGTCTG
bm-F	CATGCCATGGATGAAGTTCAGCTGGTGCAGTCAG
h-R/bm-R	CCCAAGCTTTCA*ATGGTGATGGTGATGGTG*TTTGATCTCCACCTTGGTCC

Saturated site-directed mutagenesis of humanized scFv

The residues in HCDR3 and LCDR3 are most likely to dominate the antibody-antigen interaction (Sundberg et al. 2002). To further identify critical residues involved in hPCSK9 binding, alanine scanning mutagenesis was carried out in these two regions. Briefly, residues in HCDR3 and LCDR3 excepting (a) Tyr and Trp which are advantageous for large van der Waals or hydrophobic interactions, (b) Asn and Ser which mainly form hydrogen bonds, (c) glutamine at the 89th and 90th position of the light chain (H et al. 2015), were selected to mutate to alanine. The oligonucleotide primers used were listed in Table S1. The effect of each mutated site on the activity of humanized scFv was determined by measuring the changes in LDL uptake after treating HepG2 cells with purified humanized scFv proteins. Afterwards, the key residues were identified and site-directed saturation mutagenesis was conducted on these residues using the primers listed in Table S2.

Generation of full-length antibodies

To generate full-length antibodies, the V_H and V_L of humanized scFvs were fused with the constant region of modified human IgG1 heavy chain (HC) and human kappa light chain (LC, Accession number: ABU90709.2) by overlap-extension PCR (OE-PCR) (Lu et al. 2018), respectively. Primers used for OE-PCR were listed in Table 3. The modified human IgG1 constant region contains several mutations (L234A/L235A/N297G), known to eliminate antibody-dependent cellular cytotoxicity (ADCC) and complement-dependent cellular cytotoxicity (CDC) effects (Wines et al. 2000, Hessell et al. 2007, Jefferis 2009, Jacobsen et al. 2017). The C-terminal lysine residue in the heavy chain was also deleted to mitigate mAb heterogeneity caused by C-terminal lysine incomplete cleavage (Dick et al. 2008, Liu et al. 2008). The amplified full-length HC and LC genes containing a Kozak consensus sequence (Hernández 2019) followed by a secretion signal peptide sequence

('MDWTWRFLFVVAAATGVQS' for HC secretory expression, Accession number: CAA34971.1; 'MDMRVPAQLLGLLLLWLSGARC' for LC secretory expression, Accession number: S24320) at the 5'-end were then subcloned into a mammalian expression vector pTT5 at *Eco*R I/*Hin*d III restriction sites, respectively. The constructed HC and LC expression plasmids (Fig. S7) were co-transfected into CHO-3E7 mammalian cells at a 1:1 ratio (w:w) for transient expression (Stuible 2018), and the supernatants were purified with a protein A column (Roche, Mannheim, Germany).

Table 3
PCR primers for amplification of full-length antibodies

Primer	Sequence (5'-3')
H-F0	CCGGAATTCGCCGCCACCATGGATTGGACCTGGAGATTTCTGTTTGTGGTGGCCGCCGCCACAGGC
H-F1	TTCTGTTTGTGGTGGCCGCCGCCACAGGCGTGCAGTCTCAGGTGCAGCTGGTGCAGTCTGG
H-R1	CACGGATGGGCCCTTTGTGCTGGCCGAGGAGACGGTGACCAGGGTCC
H-F2	GGACCCTGGTCACCGTCTCCTCGGCCAGCACAAAGGGCCCATCCGTG
H-R2	CCCAAGCTTTGGATACAGTTGGTGCAGCATCAGCCCGTTTC
L-F0	CCGGAATTCGCCGCCACCATGGACATGAGGGTGCCAGCTCAGCTGCTGGGACTGCTGCTGCTGTGGC
L-F1	CAGCTGCTGGGACTGCTGCTGCTGTGGCTGTCCGGAGCTAGGTGCGATATTGTGATGACCCAGTCTCC
L-R1	CTTGGAGCGGCCACGGTTCTTTTGATCTCCACCTTGGTCC
L-F2	GGACCAAGGTGGAGATCAAAAGAACCGTGGCCGCTCCAAG
L-R2	CCCAAGCTTTGGATACAGTTGGTGCAGCATCAGCC

Binding Affinity Measurement

ForteBio Octet QK^{e} (ForteBio, Fremont, CA, USA), a biomacromolecule interaction analysis system was used to measure the affinity constants of antibodies. According to the manufacturer's instruction, hPCSK9 (50 μg/ml) was biotinylated at room temperature for 2h using a biotinylation kit (Genemore, Shanghai, China) and immobilized on the surface of streptavidin biosensors (ForteBio) for 300 s. The antigen-captured biosensors were then dipped into two-fold series dilution of antibodies for 300 s or longer (association phase) and moved to SD buffer (PBS, pH 7.4, 0.02% Tween 20, 0.1% BSA) without antibodies for 600 s (dissociation phase). The concentrations of scFvs were 6000, 3000, 1500, 750, 375, 187.5, 93.75 nM, and mAbs were 800, 400, 200, 100, 50, 25, and 12.5 nM. The kinetic constants including k_{on}, k_{off}, and K_D were analyzed by using ForteBio data analysis software ver. 7.1.

Homology modeling and protein contact identification

To explore the specific binding mechanism of the antigen-antibody, the three-dimensional (3D) structure model of the Fab fragment of h5E12-L230G was constructed by SWISS-MODEL Workspace (http://swissmodel.expasy.org/) based on the top-ranked template with known structure, and the stereochemical property was checked through the Ramachandran plot (Bienert et al. 2017, Waterhouse et al. 2018). Subsequently, the constructed models were further refined and docked with a high-resolution 2.3 Å crystal structure of PCSK9 (PDB ID:5OCA) using the BioLuminate module of Schrödinger Software Suite

2009(Schrödinger). Follow this, the key interaction residues between the antibody and PCSK9 were identified using the Pymol software Version 2.3.0 (Schrödinger), and the free binding energy ($\triangle G_{binds}$) of the Fab-PCSK9-complex were evaluated using the Molecular Mechanics/GB Surface Area (MM/GBSA) method as implemented in HawkDock web server (http://cadd.zju.edu.cn/hawkdock/) (Weng et al. 2019).

Studies in mice

Male C57BL/6 mice aged 6-8 weeks were obtained from Qinglongshan Experimental Animal Breeding Farm (Certificate no. SCXK (Su) 2017-0001; Nanjing, China) and maintained on a 12-h light/dark cycle at room temperature with access to food and water ad libitum. Following 1 week of acclimation, mice were randomly split into 8 groups (a normal group, a model group, and six treatment groups, n=6 per group). On day 1, the model group and dosing group were injected 2 ml saline containing 50 μg pTT5-hPCSK9 intravenously in 5-7s to establish hyperlipidemic mouse model (Miao et al. 2001, Suda et al. 2007), while the normal group was just injected with 2 ml saline. On day 7, the dosing groups were administered with 1, 3, and 10 mg/kg of mAbs in 100 μl saline, respectively, while the normal and model groups were administered same-volume saline. Then the mice were fasted for 8 h and euthanized for blood sample collection. Liver tissues were also collected, and dissected into two parts, one was homogenized by RIPA buffer containing 1mM PMSF for western blot analysis, the other part was fixed in 4% (w/v) paraformaldehyde and embedded in paraffin for immunofluorescence analysis.

Immunofluorescence analysis

Immunofluorescence staining was performed to detect LDLR protein levels in mice livers as previously described (Gu 2019, Xu 2020) with minor modification. Briefly, after deparaffinization and hydration, liver tissue sections were pretreated by heating for 20 min in boiling sodium citrate solution (0.01 M, pH 6.0) for antigen retrieval. Thereafter, the tissue sections were blocked with 10% (v/v) goat serum in PBST for 1 h and incubated with rabbit anti-LDLR antibody (Cat# ab52818, 1:100) overnight at 4°C. After washing three times with PBS, the sections were incubated with Alexa Fluor® 488-conjugated goat anti-rabbit IgG (Cat# D110061, 1:200) at 37℃ for 1 h in the dark and the stained sections were mounted with a drop of glycerin. Images were taken under a Zeiss AX10 fluorescence microscopy (Zeiss, Oberkochen, Germany).

Statistical analysis

Data are expressed as the mean ± SEM of multiple experiments. Comparison between groups was performed using one-way analysis of variance followed by a Tukey multiple comparison test with GraphPad Prism V5.0 software. Results were considered significant when *P*-values<0.05.

Results

Generation of murine mAb against hPCSK9 by hybridoma technology

To generate murine mAb against hPCSK9, the recombinant hPCSK9 protein as the antigen was expressed by transient transfection of the pTT5-hPCSK9 plasmid (Fig. 1a) to CHO 3E7 cells and purified by Ni-IMAC, followed by a Superdex™ 200 HR 10/300GL size-exclusion chromatography. Purified hPCSK9 was then identified by 10% (w/v) SDS-PAGE (Fig. 1b) under reducing condition and Western blot (Fig. 1c) using the rabbit anti-human PCSK9 antibody (Cat# ab181142, 1:3000).

Subsequently, BALB/c mice were immunized with purified hPCSK9 protein. On day 38, the mice attaining antibody titer of 1:640000 (Fig. 1d) were sacrificed, and its splenocytes were fused with SP2/0 cells for hybridoma production. A positive hybridoma clone, named 5E12, was identified by ELISA (Fig. 1e) and subcloned three times by limiting dilution. This hPCSK9-specific murine antibody (named m5E12) was then purified from mouse ascites by protein A affinity chromatography (Roche, Mannheim, Germany) and identified by SDS-PAGE under reducing and nonreducing conditions (Fig. 1f). The purified m5E12 was analyzed by Shodex PROTEIN KW-802.5 (SHOWA DENKO K.K., Japan) showing a purity of 99% (Fig. S1).

Characterization of generated m5E12

Firstly, we determined the isotype of m5E12 using a commercial murine antibody isotyping kit (KMI-2, ProteinTech Group, Chicago, IL, USA) according to the manufacturer's instructions. The result showed that m5E12 belonged to the subtype IgG1 and the light chain of the mAb was kappa (Fig. S2). Secondly, the specificity and affinity (K_{aff}) of m5E12 to hPCSK9 were analyzed by Western blot (Fig. 2A) and ELISA (Fig. 2b). The results revealed that hPCSK9 protein could be specifically recognized by m5E12 (Fig. 2a) and the affinity constant (K_{aff}) of m5E12 to hPCSK9 protein was 1.04×10^{9} M^{-1} (Fig. 2b). Finally, we tested the effects of m5E12 on the expression levels of LDLR and LDL-C uptake in HepG2 cells. As shown in Fig. 2c and 2d, m5E12 effectively elevated the levels of LDLR and promoted the LDL-C uptake in HepG2 cells as compared to the hPCSK9 treated group.

Humanization of murine 5E12 scFv (m5E12scFv)

For antibody humanization, the V_H (Fig. 3a) and V_L (Fig. 3b) amino acid sequences of m5E12 were determined by RT-PCR and gene sequencing. The V_H and V_L of m5E12 were then linked in a format of V_H-(Gly4Ser)3-V_L, named m5E12scFv. Afterward, humanization of m5E12scFv was accomplished by CDR grafting without (named h5E12scFv) or with back mutation (h5E12scFv-bm) by modeling.

In detail, one of the humanized variable fragments, named h5E12scFv, was designed by grafting the CDRs of m5E12 onto the heavy chain (GenBank accession number: AMK70123.1) and light chain (GenBank accession number: APZ85158.1) of human antibodies (Fig. 3a and 3b). Back-mutation was then performed on h5E12scFv. On the one hand, N97 at the heavy chain and E45, R63, V78 at the light chain of the two human templates were rare residues and were mutated to corresponding conserved residues. On the other hand, the three-dimensional (3D) structures of m5E12scFv (Fig. 3c), h5E12scFv (Fig. 3d), and h5E12scFv (Fig. 3e) were modeled by Schrodinger software based on the highest identity template crystal structure and verified by Ramachandran Plot (Fig. S3), and nine key residues (E1, K38, I48, K67, A68, V72, A79, L81, and S92) and seven key residues (I4, T8, I46, H59, E85, F87, and E100) in FRs of murine V_H and V_L, which may change CDRs conformations, were also back-mutated (named h5E12scFv-bm).

The RMSD value for the three modeled entire structures (Fig. 3c-e) was 0.724 Å. The RMSDs for five non-HCDR3 loops ranged from 0.255 Å to 0.523 Å, and the HCDR3 RMSD was 1.150 Å. Since all RMSDs were less than 1.5 Å, the three structures were considered to share the same conformation at the computer level.

Preparation and selection of humanized 5E12 scFv

To prepare humanized 5E12 scFv proteins for selection, the genes encoding m5E12scFv, h5E12scFv, and h5E12scFv-bm fragments were synthesized at Genscript Biotech (Nanjing, China), amplified by PCR (Fig. S4) and then inserted into T7 promoter driven expression vector pET-27b between *Nco* I and *Hin*d III sites (Fig. 4a). The construct was transformed in *E. coli* BL21 (DE3) cells as described. After induction with 0.2 mM IPTG at 16°C for 18 h, humanized 5E12 scFv proteins (Fig. S5) were purified by Ni-NTA affinity chromatography column.

The specificity and kinetic parameters of purified humanized 5E12 scFvs binding to hPCSK9 were further determined by Competitive ELISA and Bio-Layer Interferometry (BLI) using a ForteBio Octet QK^e System. As shown in Fig. 4b, both h5E12scFv and h5E12scFv-bm could competitively react with hPCSK9, but the binding ability of h5E12scFv-bm was relatively weaker than h5E12scFv. It was further observed by BLI (Table S3) that h5E12scFv exhibited the highest affinity (K_D =1.71×10^{-7} M) to hPCSK9 with slower dissociation rate (k_{off} = 1.08×10^{-3} s^{-1}) than that of m5E12scFv (k_{off} = 7.44×10^{-3} s^{-1}) and h5E12scFv-bm (k_{off} = 1.00×10^{-2} s^{-1}), which is closely related with the lifetime of the drug-target complex (Copeland 2010, Vauquelin et al. 2010).

Additionally, we tested the effects of humanized 5E12 scFvs on the expression levels of LDLR and LDL-C uptake in HepG2 cells. As shown in Fig. 4c and 4d, h5E12scFv potently elevated the levels of LDLR and enhanced the LDL-C uptake in HepG2 cells as compared to the hPCSK9 group, but there is still a certain gap (Fig. 4d) compared with the scFv form of Alirocumab (named Ali-scFv).

Affinity maturation of h5E12scFv in vitro

To further enhance the affinity and bioactivity of h5E12scFv, we firstly identified the critical residues by alanine-scanning mutagenesis of several residues including F99, H100, D102, D104, F106, D107, R227, P229, L230, T231, respectively, and 10 mutants (Fig. 5a) named h5E12scFv-F99A, h5E12scFv-H100A, h5E12scFv-D102A, h5E12scFv-D104A, h5E12scFv-F106A, h5E12scFv-D107A, h5E12scFv-R227A, h5E12scFv-P229A, h5E12scFv-L230A and h5E12scFv-T231A were purified (data not shown). The biological activity of these mutants was compared by measuring the changes of LDL uptake using HepG2 cell-based assay. The results (Fig. 5b) showed that h5E12scFv-D102A and h5E12scFv-D107A exhibited scarcely any PCSK9 inhibitory effect, indicating that D102 and D107 was an essential residue for maintaining h5E12scFv' activity and should be retained. Besides, h5E12scFv-L230A displayed stronger biological activity than parental antibody h5E12scFv, suggesting that the mutation of L230 to other residues might improve the hPCSK9 inhibitory effect of h5E12scFv.

Secondly, site-saturated mutagenesis experiments were carried out on the L230 residue of h5E12scFv, and the corresponding mutants (Fig. S6) were purified and screened by LDL uptake assay (Fig. 5c). It was shown that the LDL uptake levels were effectively enhanced by h5E12scFv-L230A, h5E12scFv-L230S and h5E12scFv-L230G, and the LDL uptake levels in these three groups were restored to the comparable levels as in the Ali-scFv group. Thus, we chose h5E12scFv-L230A, h5E12scFv-L230S, and h5E12scFv-L230G for further construction of the full-length antibodies and *in vivo* functional studies.

Generation and characterization of full-length anti-PCSK9 antibodies

The full-length format of anti-PCSK9 antibodies was constructed by fusing the V_H and V_L with a modified human IgG1 heavy-chain constant region and kappa light chain constant region, respectively. The heavy (GenBank accession number: MW715631) and light chain DNA sequence (GenBank accession number: MW715632,

MW725291, MW725292, MW725293) of full-length antibodies were then inserted into the pTT5 vector (Fig. S7) and co-transfected into CHO-3E7 cells for transient expression. After purification by protein A affinity chromatography columns, the obtained mAbs were verified by SDS-PAGE under non-reducing and reducing conditions (Fig. 6a).

Subsequently, Dil-LDL uptake assay was performed as described above to test the hPCSK9 inhibitory effect of purified mAbs. The results (Fig. 6b) showed that all the generated mAbs, including h5E12, h5E12-L230A, h5E12-L230S, h5E12-L230G, could significantly inhibit PCSK9-induced decrease in Dil-LDL uptake of HepG2 cells (P<0.001). Among them, h5E12-L230G exhibited the most potent activity in enhancing the LDL-C uptake levels, which was comparable to the positive control Alirocumab.

We further detect and compare the affinity constant of h5E12-L230G and Alirocumab to hPCSK9 using the ForteBio Octet QK^e system. As shown in Fig. 6c, d and Table S4, h5E12-L230G displayed a moderate slower association rate (k_{on}= 2.81 × 10^4 $M^{-1}s^{-1}$) and a slightly slower dissociation rate (k_{off} = 4.84 × 10^{-5} s^{-1}) than Alirocumab (k_{on}= 8.04 × 10^4 $M^{-1}s^{-1}$, k_{off} = 6.87 × 10^{-5} s^{-1}), thus yielding a ~2-fold lower affinity (K_D = 1.72 × 10^{-9} M *vs.* 8.54 × 10^{-10} M) as compared to Alirocumab. It can be concluded that the slower dissociation rate (k_{off}) between h5E12-L230G and hPCSK9 results in a longer binding period, which may enhance the hPCSK9 inhibitory of h5E12-L230G to the comparable level of Alirocumab.

In addition, to further elucidate the epitope–paratope interaction details, the 3D structure of Fab region of h5E12-L230G (Fig. S8a) was built based on the top-ranked template crystal structure (PDB ID:6DW2). Ramachandran plot (Fig. S8b) of the modeled h5E12-L230G revealed that 97.91% of the residues were in the most favorable and allowed regions, indicating that the modeled structure was suitable for the molecular docking analysis. The following docking results (Fig. 6e) suggested that h5E12-L230G binds to the catalytic domain of hPCSK9, and both the heavy-chain and light-chain variable domain contributed to protein-ligand interaction. It appeared that as many as fourteen residues (S25, T28, W33, N55, H100, D102, Y103, D107, Y108 in heavy chain and Y49, S50, Y53, R54, S56 in light chain) in h5E12-L230G and up to fourteen residues (A168, L179, E181, E197, G198, R199, V200, V202, R237, D238, K243, S246, P279, S401 in catalytic domain) in hPCSK9 involved in the interactions, forming fifteen hydrogen bonds and two ionic bonds in the binding pocket (Table S5). Finally, the binding free energy (ΔG_{bind}) of the illustrated docking mode calculated using the MM-GBSA method was as low as -54.97 kcal/mol, indicating the h5E12-L230G showed high binding strength with hPCSK9.

Hypolipidemic effect of h5E12-L230G in mice over-expressing hPCSK9

We next evaluated the lipid-lowering efficacy of h5E12-L230G in vivo. The mice over-expressing hPCSK9 was established through hydrodynamic delivery (HDD) of 50 μg naked plasmid DNA (pTT5-hPCSK9) in 2 ml normal saline. On day 6 after HDD, the mice in the treatment groups were given a single tail *i.v.* injection of h5E12-L230G with various doses. 18 hours after administration, the levels of LDLR in liver tissues were dose-dependently up-regulated as assessed by Western blot (Fig. 7b) and Immunofluorescence (Fig. 7c). Besides, it was shown that treatment with h5E12-L230G at 1, 3, and 10 mg/kg resulted in a 5.8% (P>0.05), 30.1% (P<0.01), and 36.2% (P<0.001) decrease in serum LDL-C relative to the model group, respectively (Fig. 7a and Table 4), and h5E12-L230G treatment could also significantly lowered the levels of serum total cholesterol (TC) and triglyceride (TG), but did not significantly affect serum High-density lipoprotein (HDL-C) levels (Table 4).

Table 4
Effects of h5E12-L230G on serum lipids levels in hyperlipidemic mice model

Group		Dose (mg/kg)	LDL-C (mmol/l) *(mmol/L)*	TC (mmol/l)	HDLC (mmol/L)	TG (mmol/L)
Normal group		/	0.624 ± 0.021	3.642 ± 0.161	1.417 ± 0.042	0.0921 ± 0.028
Model group		/	1.560 ± 0.037###	5.250 ± 0.212###	1.340 ± 0.036	1.351 ± 0.049###
Alirocumab group	Low dose	1	4.903 ± 0.071	1.275 ± 0.066	1.320 ± 0.052	1.274 ± 0.066
	Medium dose	3	4.650 ± 0.066**	1.417 ± 0.088	1.211 ± 0.048	1.417 ± 0.088
	High dose	10	4.276 ± 0.062***	1.287 ± 0.054	1.162 ± 0.037*	1.287 ± 0.054
FAP2M21 group	Low dose	1	4.770 ± 0.045*	1.462 ± 0.084	1.312 ± 0.026	1.199 ± 0.039
	Medium dose	3	4.658 ± 0.022**	1.333 ± 0.071	1.196 ± 0.048	1.232 ± 0.078
	High dose	10	4.469 ± 0.063***	1.257 ± 0.044	1.155 ± 0.037*	1.348 ± 0.031

Discussion

Elevated plasma LDL-C in patients with hypercholesterolemia is a well-established risk factor for CVDs. For over three decades, numerous clinical trials have firmly demonstrated the validity of LDL-C reduction in the prevention of CVD developing (Baigent et al. 2010, Silverman 2016) and LDL-C levels have been accepted as a reliable efficacy endpoint for curative assessment and drug approval (Tardif et al. 2006). Nowadays, reduction of plasma LDL-C levels with the 3-hydroxy-3-methylglutaryl-coenzyme (HMG-CoA) reductase inhibitors (statins) remains the cornerstone of lipid management for the reduction of cardiovascular (CV) events in both primary and secondary prevention (Task Force for the management of dyslipidaemias of the European Society of et al. 2011, Miller 2019). However, a significant percentage of patients cannot tolerate any statin dose or cannot reach their recommended LDL-C goals even with a high enough statin dose (Mampuya et al. 2013, Keen et al. 2014, Mancini et al. 2016). Therefore, it is necessary to explore novel drug treatments to lower LDL-C for these special patient populations.

PCSK9, a secreted protein able to induce the degradation of LDLR thereby reduce the clearance of LDL particles, has emerged as a promising target to reduce circulating LDL-C levels (Horton et al. 2009, Bergeron et al. 2015, Yang et al. 2018). Nowadays, mAbs remain one of the most promising classes of therapeutics biological targeted drugs because of its high titer, high specificity, and long half-life, and administration of PCSK9-targeting mAbs is an effective therapeutic way to suppress the interaction between PCSK9 and LDLR (He et al. 2017, Rashid et al. 2017). More recently, several mAbs targeting PCSK9, such as Evolocumab, Alirocumab (Lu et al. 2020), and LY3015014 (Kastelein et al. 2016), have been approved for clinical use or under clinic trials. In present

study, we chose Alirocumab as the positive control and expected to generate a potent anti-hPCSK9 mAb with good druggability utilizing hybridoma-based methods.

Using the hybridoma technique, we initially generated a murine mAb targeting hPCSK9 (named m5E12), which could restore PCSK9-induced LDLR degradation and inhibit LDL uptake in HepG2 cells (Fig. 2c and 2d). What needs illustration is that the humanization and affinity maturation of m5E12 here were performed using the scFv format instead of using the full-length antibody format, this is because scFv proteins can be easily obtained from *E. coli* expression system, which has the advantage of fast-growing, inexpensive and easy manipulation (Ahmad et al. 2012, Agha Amiri et al. 2017).

Specifically, to reduce the immunogenicity of mouse antibody, m5E12 was humanized by means of CDR grafting and back-mutation methods (Verhoeyen 1988, Foote 1992, Pedersen 1994, De Haard 1999), generating two humanized m5E12 (h5E12scFv and h5E12scFv-bm) in the respective scFv format. Intriguingly, although the RMSD analysis showed that the humanized scFvs converged to the same conformation (Fig. 3c-e), their affinity (K_D) and biological activity were different. It was revealed that h5E12scFv displayed a higher affinity (K_D) and hPCSK9 inhibitory effect than h5E12scFv-bm (Fig. 4b-d). Thus, we chose h5E12scFv for further study. To further improve the antibody's affinity and bioactivity, alanine scanning mutagenesis was firstly conducted on the HCDR3 and LCDR3 of h5E12scFv by one-step PCR technology (Zheng 2004). Ten residues in HCDR3 and LCDR3 were selected to mutated to alanine, and we found that the L230A variant, termed h5E12scFv-L230A, was able to restore LDL uptake to the level slightly higher than that of parental antibody h5E12scFv (Fig. 5b). Therefore, we assumed that the alteration of L230 residues in h5E12scFv might help to improve its activity, and fortunately, the following site-saturated mutagenesis experiment proved this hypothesis (Fig. 5c).

To date, the majority of therapeutic antibodies developed are full-length IgG, and the full-length IgG molecules are considered one of the most suitable formats for clinical applications (Yang et al. 2017). Therefore, the selected optimized scFv mutants (h5E12scFv-L230A, h5E12scFv-L230G, h5E12scFv-L230S) were then reformatted into full-length Fc-silenced IgG1 format (Wines 2000, Hessell 2007, Dick 2008, Liu 2008, Jefferis 2009, Jacobsen 2017), expressed transiently in CHO mammalian cells and purified from culture supernatant. Of these full-length antibodies, h5E12-L230G could reverse LDL uptake to the similar levels of Alirocumab (Fig. 6b) and bind to hPCSK9 with a 1.41-fold slower dissociation rate (k_{off} = 4.84 × 10^{-5} s^{-1}) than Alirocumab (k_{off} = 6.87 × 10^{-5} s^{-1}).

Molecular Modeling and docking techniques are wildly used to predict the binding mode of an antibody with its protein target (Kosztyu et al. 2019, Vahed et al. 2020). In this work, the docking results (Fig. 6e and Table S5) showed that up to fourteen amino acid residues in h5E12-L230G form the paratope that interacts with fourteen amino acid residues in hPCSK9's epitope, creating as many as fifteen hydrogen bonds and two ionic bonds on the interaction site. Hence, the multiple interactions between the CDRs of h5E12-L230G and the catalytic domain of PCSK9 resulted in a tight binding of h5E12-L230G to hPCSK9, which might well explain the excellent PCSK9 inhibitory activity of h5E12-L230G.

It is also remarkable that a targeted therapeutic drug requires a long period on the target to be effective, hence the fairly slow dissociation rate of h5E12-L230G to hPCSK9 is desirable to facilitate prolonged duration of antibody-antigen interaction and is especially important for its *in vivo* targeting applications (Axworthy et al. 2000, Chmura et al. 2001, Bottermann et al. 2016). As expected, h5E12-L230G showed considerable potency in raising LDLR expression in mice liver (Fig. 7b) and effectively reduced serum LDL-C and TC levels in

hyperlipidemic C57BL/6 mice in a dose-dependent manner (Table 4), with high potency comparable to the positive control Alirocumab.

In conclusion, h5E12-L230G is a humanized high-affinity hPCSK9 blocking antibody which binds to the catalytic domain of hPCSK9 with a slow dissociation rate and effectively inhibits PCSK9-mediated LDLR degradation, thereby significantly promotes LDL-C uptake in HepG2 cells and reduces the serum LDL-C and total cholesterol (TC) levels in hyperlipidemic mouse model. The data demonstrate that h5E12-L230G has the potential to serve as a therapeutic antibody targeting PCSK9 for treating hypercholesterolemia and relevant cardiovascular diseases.

Abbreviations

CDR, complementarity-determining region; CHO, Chinese hamster ovary cells; CVDs, cardiovascular diseases; DMEM, Dulbecco's modified Eagle's medium; *Escherichia coli*, *E. Coli*. ELISA, Enzyme-linked immunosorbent assay; FBS, fetal bovine serum. HC, heavy chain; HDL-C, High-density lipoprotein receptor; IPTG, isopropyl-β-galactosidase. LDLR, low-density lipoprotein receptor; LDL-C, low-density lipoprotein cholesterol; LC, light chain; MM/GBSA, Molecular Mechanics/GB Surface Area; mAb, Monoclonal antibody; PCSK9, Proprotein convertase subtilisin/kexin type 9; RMSD, Root mean square deviation; scFv, single-chain variable fragment; TC, total cholesterol; TG, triglyceride; VH, variable region of heavy chain; VL, variable region of light chain.

Declarations

Ethics approval and consent to participate

Experiments were performed under a project license (NO.: 201601179) granted by the Animal Ethics Committees of China Pharmaceutical University, in compliance with national guidelines for the care and use of animals.

Consent to participate

Not applicable.

Consent for publication

Authors consent to publish with no conflict of interest.

Availability of data and materials

All data generated or analysed during this study are included in this manuscript and supplementary information.

Competing interests

The authors have no conflicts of interest to declare.

Funding

This work was funded by National Fund for Major Projects of China (2009ZX09103-653; 2013ZX09301303-006; 2018ZX09301035), The Priority Academic Program Development of Jiangsu Higher Education Institutions

(PAPD), National Fund for Fostering Talents of Basic Science (NFFTBS, 3050040016), China Pharmaceutical University “Double First-Class” project (CPU2018GY15).

Authors’ contributions

S. Tan conceptualized the project and reviewing the manuscript. Z. Bai planned for the project, performed the hybridoma experiment and wrote the first draft of the manuscript. M. Xu designed research and edited the manuscript. Y. Mei performed the humanization experiment and participated in drafting the article. T. Hu purified the antibodies, analyzed the data and co-wrote the manuscript. P. Zhang helped Y. Mei and T. Hu with analysis of molecular modeling and docking studies. M. Chen expressed and purified the antigen. W. Lv helped M. Chen in antigen preparation. C. Lu preparation the antigen.

Acknowledgements

Not applicable.

References

1. Abifadel, M., M. Varret, J. P. Rabes, D. Allard, K. Ouguerram, M. Devillers, C. Cruaud, S. Benjannet, L. Wickham, D. Erlich, A. Derre, L. Villeger, M. Farnier, I. Beucler, E. Bruckert, J. Chambaz, B. Chanu, J. M. Lecerf, G. Luc, P. Moulin, J. Weissenbach, A. Prat, M. Krempf, C. Junien, N. G. Seidah and C. Boileau (2003). "Mutations in PCSK9 cause autosomal dominant hypercholesterolemia." Nat Genet 34(2): 154-156. DOI:10.1038/ng1161
2. Agha Amiri, S., S. Shahhosseini, N. Zarei, D. Khorasanizadeh, E. Aminollahi, F. Rezaie, M. Zargari, M. Azizi and V. Khalaj (2017). "A novel anti-CD22 scFv-apoptin fusion protein induces apoptosis in malignant B-cells." AMB Express 7(1): 112. DOI:10.1186/s13568-017-0410-5
3. Ahmad, Z. A., S. K. Yeap, A. M. Ali, W. Y. Ho, N. B. Alitheen and M. Hamid (2012). "scFv antibody: principles and clinical application." Clin Dev Immunol 2012: 980250. DOI:10.1155/2012/980250
4. Axworthy, D. B., J. M. Reno, M. D. Hylarides, R. W. Mallett, L. J. Theodore, L. M. Gustavson, F. M. Su, L. J. Hobson, P. L. Beaumier and A. R. Fritzberg (2000). "Cure of human carcinoma xenografts by a single dose of pretargeted yttrium-90 with negligible toxicity." Proceedings of the National Academy of Sciences 97(4): 1802. DOI:10.1073/pnas.97.4.1802
5. Baigent, C., L. Blackwell, J. Emberson, L. E. Holland, C. Reith, Bhala, N., , R. Peto, Barnes, E., K. H., A., , J. Simes and R. Collins (2010). "Efficacy and safety of more intensive lowering of LDL cholesterol: a meta-analysis of data from 170 000 participants in 26 randomised trials." The Lancet 376(9753): 1670-1681. DOI:10.1016/s0140-6736(10)61350-5
6. Beatty, J. D., B. G. Beatty and W. G. Vlahos (1987). "Measurement of monoclonal antibody affinity by non-competitive enzyme immunoassay." J Immunol Methods 100(1): 173-179. DOI:https://doi.org/10.1016/0022-1759(87)90187-6
7. Bergeron, N., B. A. Phan, Y. Ding, A. Fong and R. M. Krauss (2015). "Proprotein convertase subtilisin/kexin type 9 inhibition: a new therapeutic mechanism for reducing cardiovascular disease risk." Circulation 132(17): 1648-1666. DOI:10.1161/CIRCULATIONAHA.115.016080
8. Bienert, S., A. Waterhouse, T. A. de Beer, G. Tauriello, G. Studer, L. Bordoli and T. Schwede (2017). "The SWISS-MODEL Repository-new features and functionality." Nucleic Acids Res 45(D1): D313-D319.

DOI:10.1093/nar/gkw1132

9. Blanco-Toribio, A., A. Alvarez-Cienfuegos, N. Sainz-Pastor, N. Merino, M. Compte, L. Sanz, F. J. Blanco and L. Alvarez-Vallina (2015). "Bacterial secretion of soluble and functional trivalent scFv-based N-terminal trimerbodies." AMB Express 5(1): 137. DOI:10.1186/s13568-015-0137-0
10. Bottermann, M., H. E. Lode, R. E. Watkinson, S. Foss, I. Sandlie, J. T. Andersen and L. C. James (2016). "Antibody-antigen kinetics constrain intracellular humoral immunity." Sci Rep 6: 37457. DOI:10.1038/srep37457
11. Brown, M. S. and J. L. Goldstein (1986). "A receptor-mediated pathway for cholesterol homeostasis." Science 232(4746): 34-47. DOI:10.1126/science.3513311
12. Chan, K. T., S. C. Cheng, H. Xie and Y. Xie (2001). "A humanized monoclonal antibody constructed from intronless expression vectors targets human hepatocellular carcinoma cells." Biochem Biophys Res Commun 284(1): 157-167. DOI:10.1006/bbrc.2001.4837
13. Chiu, M. L. and G. L. Gilliland (2016). "Engineering antibody therapeutics." Curr Opin Struct Biol 38: 163-173. DOI:10.1016/j.sbi.2016.07.012
14. Chmura, A. J., M. S. Orton and C. F. Meares (2001). "Antibodies with infinite affinity." Proc Natl Acad Sci U S A 98(15): 8480-8484. DOI:10.1073/pnas.151260298
15. Cohen, J. C., E. Boerwinkle, T. H. Mosley, Jr. and H. H. Hobbs (2006). "Sequence variations in PCSK9, low LDL, and protection against coronary heart disease." N Engl J Med 354(12): 1264-1272. DOI:10.1056/NEJMoa054013
16. Copeland, R. A. (2010). "The dynamics of drug-target interactions: drug-target residence time and its impact on efficacy and safety." Expert Opinion on Drug Discovery 5(4): 305-310. DOI:10.1517/17460441003677725
17. Cunningham, D., D. E. Danley, K. F. Geoghegan, M. C. Griffor, J. L. Hawkins, T. A. Subashi, A. H. Varghese, M. J. Ammirati, J. S. Culp, L. R. Hoth, M. N. Mansour, K. M. McGrath, A. P. Seddon, S. Shenolikar, K. J. Stutzman-Engwall, L. C. Warren, D. Xia and X. Qiu (2007). "Structural and biophysical studies of PCSK9 and its mutants linked to familial hypercholesterolemia." Nat Struct Mol Biol 14(5): 413-419. DOI:10.1038/nsmb1235
18. De Haard, H., B. Kazemier, V. D. B. Arie, P. Oudshoorn, P. Boender, J. W. Arends and B. J. I. Van Gemen (1999). "Vernier zone residue 4 of mouse subgroup II kappa light chains is a critical determinant for antigen recognition." Immunotechnology 4(3-4): 203-215.
19. Dick, L. W., Jr., D. Qiu, D. Mahon, M. Adamo and K. C. Cheng (2008). "C-terminal lysine variants in fully human monoclonal antibodies: investigation of test methods and possible causes." Biotechnology and Bioengineering 100(6): 1132-1143. DOI:10.1002/bit.21855
20. Egom, E. E., R. B. Pharithi, S. Hesse, N. Starr, R. Armstrong, H. M. Sulaiman, K. Gazdikova, I. Mozos, M. Caprnda, P. Kubatka, P. Kruzliak, B. Khan, L. Gaspar and V. M. G. Maher (2019). "Latest Updates on Lipid Management." High Blood Press Cardiovasc Prev 26(2): 85-100. DOI:10.1007/s40292-019-00306-8
21. Elgundi, Z., M. Reslan, E. Cruz, V. Sifniotis and V. Kayser (2017). "The state-of-play and future of antibody therapeutics." Adv Drug Deliv Rev 122: 2-19. DOI:10.1016/j.addr.2016.11.004
22. Ersching, J., A. Efeyan, L. Mesin, J. T. Jacobsen, G. Pasqual, B. C. Grabiner, D. Dominguez-Sola, D. M. Sabatini and G. D. Victora (2017). "Germinal Center Selection and Affinity Maturation Require Dynamic Regulation of mTORC1 Kinase." Immunity 46(6): 1045-1058 e1046. DOI:10.1016/j.immuni.2017.06.005

23. Farnier, M. (2018). "Lowering low-density lipoprotein cholesterol by PCSK9 inhibition in patients with diabetes on insulin therapy: is it efficacious and safe?" Ann Transl Med 6(3): 60. DOI:10.21037/atm.2018.01.02
24. Foote, J. and G. J. J. o. M. B. Winter (1992). "Antibody framework residues affecting the conformation of the hypervariable loops." J Mol Biol 224(2): 0-499.
25. Gu, L., P. Ye, H. Li, Y. Wang, Y. Xu, Q. Tian, G. Lei, C. Zhao, Z. Gao, W. Zhao and S. Tan (2019). "Lunasin attenuates oxidant-induced endothelial injury and inhibits atherosclerotic plaque progression in ApoE(-/-) mice by up-regulating heme oxygenase-1 via PI3K/Akt/Nrf2/ARE pathway." FASEB J 33(4): 4836-4850. DOI:10.1096/fj.201802251R
26. H, A. and T. K (2015). "Thermodynamics of antibody-antigen interaction revealed by mutation analysis of antibody variable regions." Journal of Biochemistry 158(1): 1-13. DOI:10.1093/jb/mvv049
27. Haidar, J. N., Q. A. Yuan, L. Zeng, M. Snavely, X. Luna, H. Zhang, W. Zhu, D. L. Ludwig and Z. Zhu (2012). "A universal combinatorial design of antibody framework to graft distinct CDR sequences: a bioinformatics approach." Proteins 80(3): 896-912. DOI:10.1002/prot.23246
28. He, N. Y., Q. Li, C. Y. Wu, Z. Ren, Y. Gao, L. H. Pan, M. M. Wang, H. Y. Wen, Z. S. Jiang, Z. H. Tang and L. S. Liu (2017). "Lowering serum lipids via PCSK9-targeting drugs: current advances and future perspectives." Acta Pharmacol Sin 38(3): 301-311. DOI:10.1038/aps.2016.134
29. Hernández, G., V. G. Osnaya and X. Pérez-Martínez (2019). "Conservation and Variability of the AUG Initiation Codon Context in Eukaryotes." Trends in Biochemical Sciences 44(12): 1009-1021. DOI:https://doi.org/10.1016/j.tibs.2019.07.001
30. Hessell, A. J., L. Hangartner, M. Hunter, C. E. Havenith, F. J. Beurskens, J. M. Bakker, C. M. Lanigan, G. Landucci, D. N. Forthal, P. W. Parren, P. A. Marx and D. R. Burton (2007). "Fc receptor but not complement binding is important in antibody protection against HIV." Nature 449(7158): 101-104. DOI:10.1038/nature06106
31. Holla, O. L., J. Cameron, K. E. Berge, T. Ranheim and T. P. Leren (2007). "Degradation of the LDL receptors by PCSK9 is not mediated by a secreted protein acted upon by PCSK9 extracellularly." BMC Cell Biol 8: 9. DOI:10.1186/1471-2121-8-9
32. Horton, J. D., J. C. Cohen and H. H. Hobbs (2009). "PCSK9: a convertase that coordinates LDL catabolism." J Lipid Res 50 Suppl: S172-177. DOI:10.1194/jlr.R800091-JLR200
33. Inoue, H., A. Suganami, I. Ishida, Y. Tamura and Y. Maeda (2013). "Affinity maturation of a CDR3-grafted VHH using in silico analysis and surface plasmon resonance." J Biochem 154(4): 325-332. DOI:10.1093/jb/mvt058
34. Jacobsen, F. W., R. Stevenson, C. Li, H. Salimi-Moosavi, L. Liu, J. Wen, Q. Luo, K. Daris, L. Buck, S. Miller, S. Y. Ho, W. Wang, Q. Chen, K. Walker, J. Wypych, L. Narhi and K. Gunasekaran (2017). "Engineering an IgG Scaffold Lacking Effector Function with Optimized Developability." J Biol Chem 292(5): 1865-1875. DOI:10.1074/jbc.M116.748525
35. Jefferis, R. (2009). "Recombinant antibody therapeutics: the impact of glycosylation on mechanisms of action." Trends Pharmacol Sci 30(7): 356-362. DOI:10.1016/j.tips.2009.04.007
36. Kastelein, J. J., S. E. Nissen, D. J. Rader, G. K. Hovingh, M. D. Wang, T. Shen and K. A. Krueger (2016). "Safety and efficacy of LY3015014, a monoclonal antibody to proprotein convertase subtilisin/kexin type 9 (PCSK9):

a randomized, placebo-controlled Phase 2 study." Eur Heart J 37(17): 1360-1369. DOI:10.1093/eurheartj/ehv707

37. Keen, H. I., J. Krishnarajah, T. R. Bates and G. F. Watts (2014). "Statin myopathy: the fly in the ointment for the prevention of cardiovascular disease in the 21st century?" Expert Opin Drug Saf 13(9): 1227-1239. DOI:10.1517/14740338.2014.937422
38. Kim, H. Y., A. Stojadinovic and M. J. Izadjoo (2014). "Immunization, hybridoma generation, and selection for monoclonal antibody production." Methods Mol Biol 1131: 33-45. DOI:10.1007/978-1-62703-992-5_3
39. Ko, B. K., S. Choi, L. G. Cui, Y. H. Lee, I. S. Hwang, K. T. Kim, H. Shim and J. S. Lee (2015). "Affinity Maturation of Monoclonal Antibody 1E11 by Targeted Randomization in CDR3 Regions Optimizes Therapeutic Antibody Targeting of HER2-Positive Gastric Cancer." Plos One 10(7): e0134600.
40. KÖHler, G. and C. Milstein (1975). "Continuous cultures of fused cells secreting antibody of predefined specificity." Nature 256(5517): 495-497. DOI:10.1038/256495a0
41. Kosztyu, P., M. Kuchar, J. Cerny, L. Barkocziova, M. Maly, H. Petrokova, L. Czernekova, V. Liskova, L. Raskova Kafkova, P. Knotigova, J. Masek, J. Turanek, P. Maly and M. Raska (2019). "Proteins mimicking epitope of HIV-1 virus neutralizing antibody induce virus-neutralizing sera in mice." EBioMedicine 47: 247-256. DOI:10.1016/j.ebiom.2019.07.015
42. Levin, A. M. and G. A. Weiss (2006). "Optimizing the affinity and specificity of proteins with molecular display." Mol Biosyst 2(1): 49-57. DOI:10.1039/b511782h
43. Li, S., H. Shen and Q. Shu (2019). "S3Ab, a novel antibody targeting B lymphocytes, is a potential therapeutic agent for B-lineage malignancies." J Drug Target 27(10): 1053-1060. DOI:10.1080/1061186X.2019.1584809
44. Lindholm, M. W., J. Elmen, N. Fisker, H. F. Hansen, R. Persson, M. R. Moller, C. Rosenbohm, H. Orum, E. M. Straarup and T. Koch (2012). "PCSK9 LNA antisense oligonucleotides induce sustained reduction of LDL cholesterol in nonhuman primates." Mol Ther 20(2): 376-381. DOI:10.1038/mt.2011.260
45. Liu, H., G. Gaza-Bulseco, D. Faldu, C. Chumsae and J. Sun (2008). "Heterogeneity of monoclonal antibodies." J Pharm Sci 97(7): 2426-2447. DOI:10.1002/jps.21180
46. Lu, R. M., Y. C. Hwang, I. J. Liu, C. C. Lee, H. Z. Tsai, H. J. Li and H. C. Wu (2020). "Development of therapeutic antibodies for the treatment of diseases." J Biomed Sci 27(1): 1. DOI:10.1186/s12929-019-0592-z
47. Lu, Y., S. Xiao, M. Yuan, Y. Gao, J. Sun and C. Xue (2018). "Using overlap-extension PCR technique to fusing genes for constructing recombinant plasmids." J Basic Microbiol 58(3): 273-276. DOI:10.1002/jobm.201700455
48. Luo, S., X. Deng, Z. Xie, J. Huang, M. Zhang, M. Li, L. Xie, D. Li, Q. Fan, S. Wang, T. Zeng, Y. Zhang and Z. Xie (2020). "Production and identification of monoclonal antibodies and development of a sandwich ELISA for detection of the H3-subtype avian influenza virus antigen." AMB Express 10(1): 49. DOI:10.1186/s13568-020-00988-7
49. Ly, K., Y. G. Saavedra, M. Canuel, S. Routhier, R. Desjardins, J. Hamelin, J. Mayne, C. Lazure, N. G. Seidah and R. Day (2014). "Annexin A2 reduces PCSK9 protein levels via a translational mechanism and interacts with the M1 and M2 domains of PCSK9." J Biol Chem 289(25): 17732-17746. DOI:10.1074/jbc.M113.541094
50. Mampuya, W. M., D. Frid, M. Rocco, J. Huang, D. M. Brennan, S. L. Hazen and L. Cho (2013). "Treatment strategies in patients with statin intolerance: the Cleveland Clinic experience." Am Heart J 166(3): 597-603. DOI:10.1016/j.ahj.2013.06.004

51. Mancini, G. B., S. Baker, J. Bergeron, D. Fitchett, J. Frohlich, J. Genest, M. Gupta, R. A. Hegele, D. Ng, G. J. Pearson, J. Pope and A. Y. Tashakkor (2016). "Diagnosis, Prevention, and Management of Statin Adverse Effects and Intolerance: Canadian Consensus Working Group Update (2016)." Can J Cardiol 32(7 Suppl): S35-65. DOI:10.1016/j.cjca.2016.01.003
52. Miao, C. H., A. R. Thompson, K. Loeb and X. Ye (2001). "Long-term and therapeutic-level hepatic gene expression of human factor IX after naked plasmid transfer in vivo." Mol Ther 3(6): 947-957. DOI:10.1006/mthe.2001.0333
53. Mihaylova, B., J. Emberson, L. Blackwell, A. Keech, J. Simes, E. Barnes, M. Voysey, A. Gray, R. Collins and C. Baigent (2012). "The effects of lowering LDL cholesterol with statin therapy in people at low risk of vascular disease: meta-analysis of individual data from 27 randomised trials." The Lancet 380(9841): 581-590. DOI:10.1016/s0140-6736(12)60367-5
54. Miller, M. (2019). "ACC/AHA lipids & ASCVD guidelines: 2018 update." Metabolism 99: 116-118. DOI:10.1016/j.metabol.2019.03.008
55. Mitchell, T., G. Chao, D. Sitkoff, F. Lo, H. Monshizadegan, D. Meyers, S. Low, K. Russo, R. DiBella, F. Denhez, M. Gao, J. Myers, G. Duke, M. Witmer, B. Miao, S. P. Ho, J. Khan and R. A. Parker (2014). "Pharmacologic profile of the Adnectin BMS-962476, a small protein biologic alternative to PCSK9 antibodies for low-density lipoprotein lowering." J Pharmacol Exp Ther 350(2): 412-424. DOI:10.1124/jpet.114.214221
56. Morrison, S. L., M. J. Johnson, L. A. Herzenberg and V. T. Oi (1984). "Chimeric human antibody molecules: mouse antigen-binding domains with human constant region domains." Proc Natl Acad Sci U S A 81(21): 6851-6855.
57. Nassoury, N., D. A. Blasiole, A. Tebon Oler, S. Benjannet, J. Hamelin, V. Poupon, P. S. McPherson, A. D. Attie, A. Prat and N. G. Seidah (2007). "The cellular trafficking of the secretory proprotein convertase PCSK9 and its dependence on the LDLR." Traffic 8(6): 718-732. DOI:10.1111/j.1600-0854.2007.00562.x
58. Pedersen, J. T., A. H. Henry, S. J. Searle, B. C. Guild, M. Roguska and A. R. Rees (1994). "Comparison of Surface Accessible Residues in Human and Murine Immunoglobulin Fv Domains." J Mol Biol 235(3): 959-973.
59. Poirier, S., G. Mayer, V. Poupon, P. S. McPherson, R. Desjardins, K. Ly, M. C. Asselin, R. Day, F. J. Duclos, M. Witmer, R. Parker, A. Prat and N. G. Seidah (2009). "Dissection of the endogenous cellular pathways of PCSK9-induced low density lipoprotein receptor degradation: evidence for an intracellular route." J Biol Chem 284(42): 28856-28864. DOI:10.1074/jbc.M109.037085
60. Rader, D. J. and A. Daugherty (2008). "Translating molecular discoveries into new therapies for atherosclerosis." Nature 451(7181): 904-913. DOI:10.1038/nature06796
61. nature06796 [pii]
62. Rashid, H., I. T. Meredith and A. Nasis (2017). "PCSK9 Monoclonal Antibodies in 2016: Current Status and Future Challenges." Heart Lung Circ 26(8): 786-798. DOI:10.1016/j.hlc.2016.12.005
63. Ren, K., B. Wang and Q. Qi (2021). "Development of a new EGFR antibody antagonist which exhibits potential biological effects against laryngeal cancer." Ann Transl Med 9(12): 964. DOI:10.21037/atm-21-1839
64. Safdari, Y., S. Farajnia, M. Asgharzadeh and M. Khalili (2013). "Antibody humanization methods – a review and update." Biotechnology and Genetic Engineering Reviews 29(2): 175-186. DOI:10.1080/02648725.2013.801235

65. Schmit, D., D. Fliser and T. Speer (2019). "Proprotein convertase subtilisin/kexin type 9 in kidney disease." Nephrol Dial Transplant. DOI:10.1093/ndt/gfz122
66. Schwartz, G. G., L. Bessac, L. G. Berdan, D. L. Bhatt, V. Bittner, R. Diaz, S. G. Goodman, C. Hanotin, R. A. Harrington, J. W. Jukema, K. W. Mahaffey, A. Moryusef, R. Pordy, M. T. Roe, T. Rorick, W. J. Sasiela, C. Shirodaria, M. Szarek, J. F. Tamby, P. Tricoci, H. White, A. Zeiher and P. G. Steg (2014). "Effect of alirocumab, a monoclonal antibody to PCSK9, on long-term cardiovascular outcomes following acute coronary syndromes: rationale and design of the ODYSSEY outcomes trial." Am Heart J 168(5): 682-689. DOI:10.1016/j.ahj.2014.07.028
67. Sheedy, C., C. R. MacKenzie and J. C. Hall (2007). "Isolation and affinity maturation of hapten-specific antibodies." Biotechnol Adv 25(4): 333-352. DOI:10.1016/j.biotechadv.2007.02.003
68. Silverman, M. G., B. A. Ference, K. Im, S. D. Wiviott, R. P. Giugliano, S. M. Grundy, E. Braunwald and M. S. Sabatine (2016). "Association Between Lowering LDL-C and Cardiovascular Risk Reduction Among Different Therapeutic Interventions: A Systematic Review and Meta-analysis." JAMA 316(12): 1289-1297. DOI:10.1001/jama.2016.13985
69. Stroes, E., D. Colquhoun, D. Sullivan, F. Civeira, R. S. Rosenson, G. F. Watts, E. Bruckert, L. Cho, R. Dent, B. Knusel, A. Xue, R. Scott, S. M. Wasserman and M. Rocco (2014). "Anti-PCSK9 antibody effectively lowers cholesterol in patients with statin intolerance: the GAUSS-2 randomized, placebo-controlled phase 3 clinical trial of evolocumab." J Am Coll Cardiol 63(23): 2541-2548. DOI:10.1016/j.jacc.2014.03.019
70. Stuible, M., A. Burlacu, S. Perret, D. Brochu, B. Paul-Roc, J. Baardsnes, M. Loignon, E. Grazzini and Y. Durocher (2018). "Optimization of a high-cell-density polyethylenimine transfection method for rapid protein production in CHO-EBNA1 cells." J Biotechnol 281: 39-47. DOI:10.1016/j.jbiotec.2018.06.307
71. Suda, T. and D. Liu (2007). "Hydrodynamic gene delivery: its principles and applications." Mol Ther 15(12): 2063-2069. DOI:10.1038/sj.mt.6300314
72. Sundberg, E. J. and R. A. Mariuzza (2002). "Molecular recognition in antibody-antigen complexes." Adv Protein Chem 61: 119-160. DOI:10.1016/s0065-3233(02)61004-6
73. Tardif, J. C., T. Heinonen, D. Orloff and P. Libby (2006). "Vascular biomarkers and surrogates in cardiovascular disease." Circulation 113(25): 2936-2942. DOI:10.1161/CIRCULATIONAHA.105.598987
74. Task Force for the management of dyslipidaemias of the European Society of, C., S. the European Atherosclerosis, A. L. Catapano, Z. Reiner, G. De Backer, I. Graham, M. R. Taskinen, O. Wiklund, S. Agewall, E. Alegria, M. J. Chapman, P. Durrington, S. Erdine, J. Halcox, R. Hobbs, J. Kjekshus, P. Perrone Filardi, G. Riccardi, R. F. Storey, D. Wood, E. S. C. C. f. P. Guidelines and Committees (2011). "ESC/EAS Guidelines for the management of dyslipidaemias: the Task Force for the management of dyslipidaemias of the European Society of Cardiology (ESC) and the European Atherosclerosis Society (EAS)." Atherosclerosis 217 Suppl 1: S1-44. DOI:10.1016/j.atherosclerosis.2011.06.012
75. Tietge, U. J. (2014). "Hyperlipidemia and cardiovascular disease: inflammation, dyslipidemia, and atherosclerosis." Curr Opin Lipidol 25(1): 94-95. DOI:10.1097/MOL.0000000000000051
76. 00041433-201402000-00016 [pii]
77. Timms, K. M., S. Wagner, M. E. Samuels, K. Forbey, H. Goldfine, S. Jammulapati, M. H. Skolnick, P. N. Hopkins, S. C. Hunt and D. M. Shattuck (2004). "A mutation in PCSK9 causing autosomal-dominant hypercholesterolemia in a Utah pedigree." Hum Genet 114(4): 349-353. DOI:10.1007/s00439-003-1071-9

78. Vahed, M., F. Ramezani, V. Tafakori, V. S. Mirbagheri, A. Najafı and G. Ahmadian (2020). "Molecular dynamics simulation and experimental study of the surface-display of SPA protein via Lpp-OmpA system for screening of IgG." AMB Express 10(1): 161. DOI:10.1186/s13568-020-01097-1
79. van Poelgeest, E. P., M. R. Hodges, M. Moerland, Y. Tessier, A. A. Levin, R. Persson, M. W. Lindholm, K. Dumong Erichsen, H. Orum, A. F. Cohen and J. Burggraaf (2015). "Antisense-mediated reduction of proprotein convertase subtilisin/kexin type 9 (PCSK9): a first-in-human randomized, placebo-controlled trial." Br J Clin Pharmacol 80(6): 1350-1361. DOI:10.1111/bcp.12738
80. Vauquelin, G. and S. J. Charlton (2010). "Long-lasting target binding and rebinding as mechanisms to prolong in vivo drug action." Br J Pharmacol 161(3): 488-508. DOI:10.1111/j.1476-5381.2010.00936.x
81. Verhoeyen, M., C. Milstein and G. Winter (1988). "Reshaping human antibodies: grafting an antilysozyme activity." Science 239(4847): 1534-1536. DOI:10.1126/science.2451287
82. Wang, Z., M. Raifu, M. Howard, L. Smith, D. Hansen, R. Goldsby and D. Ratner (2000). "Universal PCR amplification of mouse immunoglobulin gene variable regions: the design of degenerate primers and an assessment of the effect of DNA polymerase 3' to 5' exonuclease activity." J Immunol Methods 233(1-2): 167-177. DOI:10.1016/s0022-1759(99)00184-2
83. Waterhouse, A., M. Bertoni, S. Bienert, G. Studer, G. Tauriello, R. Gumienny, F. T. Heer, T. A. P. de Beer, C. Rempfer, L. Bordoli, R. Lepore and T. Schwede (2018). "SWISS-MODEL: homology modelling of protein structures and complexes." Nucleic Acids Res 46(W1): W296-W303. DOI:10.1093/nar/gky427
84. Weng, G., E. Wang, Z. Wang, H. Liu, F. Zhu, D. Li and T. Hou (2019). "HawkDock: a web server to predict and analyze the protein-protein complex based on computational docking and MM/GBSA." Nucleic Acids Res 47(W1): W322-W330. DOI:10.1093/nar/gkz397
85. Wines, B. D., M. S. Powell, P. W. Parren, N. Barnes and P. M. Hogarth (2000). "The IgG Fc contains distinct Fc receptor (FcR) binding sites: the leukocyte receptors Fc gamma RI and Fc gamma RIIa bind to a region in the Fc distinct from that recognized by neonatal FcR and protein A." J Immunol 164(10): 5313-5318. DOI:10.4049/jimmunol.164.10.5313
86. Wu, N. Q. and J. J. Li (2014). "PCSK9 gene mutations and low-density lipoprotein cholesterol." Clin Chim Acta 431(3): 148-153. DOI:10.1016/j.cca.2014.01.043
87. Xu, Y., J. Gao, Y. Gong, M. Chen, J. Chen, W. Zhao and S. Tan (2020). "Hsa-miR-140-5p down-regulates LDL receptor and attenuates LDL-C uptake in human hepatocytes." Atherosclerosis 297: 111-119. DOI:10.1016/j.atherosclerosis.2020.02.004
88. Yang, C., X. Gao and R. Gong (2017). "Engineering of Fc Fragments with Optimized Physicochemical Properties Implying Improvement of Clinical Potentials for Fc-Based Therapeutics." Front Immunol 8: 1860. DOI:10.3389/fimmu.2017.01860
89. Yang, X., J. Zhang, L. Chen, Q. Wu and C. Yu (2018). "Chitosan oligosaccharides enhance lipid droplets via down-regulation of PCSK9 gene expression in HepG2 cells." Exp Cell Res 366(2): 152-160. DOI:10.1016/j.yexcr.2018.03.013
90. Yokote, K., S. Kanada, O. Matsuoka, H. Sekino, K. Imai, J. Tabira, N. Matsuoka, S. Chaudhuri and T. Teramoto (2017). "Efficacy and Safety of Bococizumab (RN316/PF-04950615), a Monoclonal Antibody Against Proprotein Convertase Subtilisin/Kexin Type 9, in Hypercholesterolemic Japanese Subjects Receiving a Stable Dose of Atorvastatin or Treatment-Naive- Results From a Randomized, Placebo-Controlled, Dose-Ranging Study." Circ J 81(10): 1496-1505. DOI:10.1253/circj.CJ-16-1310

91. Yun, S., S. Lee, J. P. Park, J. Choo and E. K. Lee (2019). "Modification of phage display technique for improved screening of high-affinity binding peptides." J Biotechnol 289: 88-92. DOI:10.1016/j.jbiotec.2018.11.020
92. Zheng, L. (2004). "An efficient one-step site-directed and site-saturation mutagenesis protocol." Nucleic Acids Res 32(14): e115. DOI:10.1093/nar/gnh110

Figures

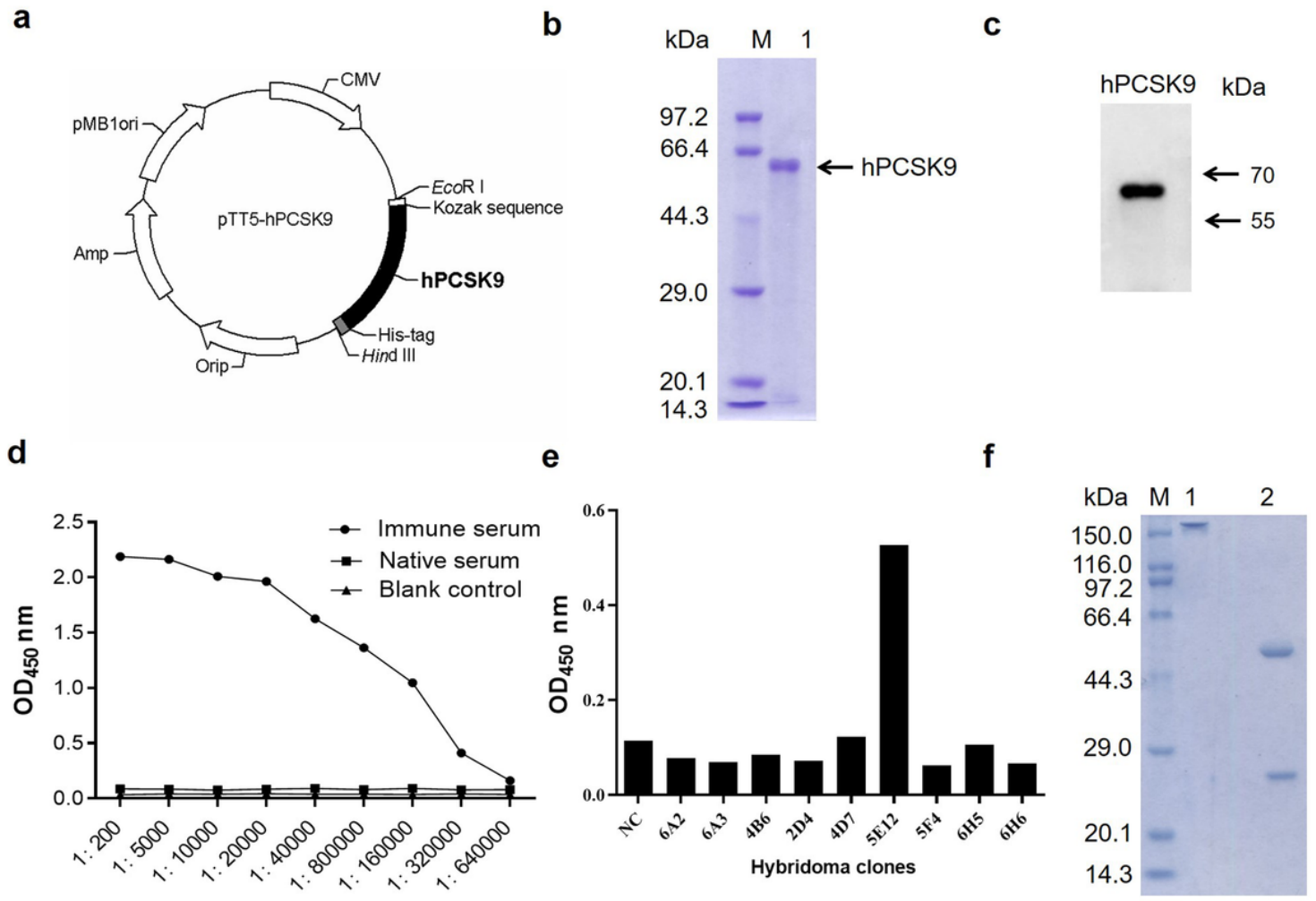

Figure 1

Generation of murine mAb against hPCSK9 protein. (a) Schematic representation of plasmid expressing hPCSK9. Kozak, Kozak consensus sequence; hPCSK9, the full-length sequence of human PCSK9 (GenBank accession number: NM_174936.3). (b) 10% (w/v) SDS-PAGE analysis of purified hPCSK9. M, molecular weight marker; Lane 1, purified hPCSK9 protein. There was a major band of 62 kDa corresponding to the catalytic and C-terminal domains of hPCSK9. (c) Purified hPCSK9 was identified by Western blot using the rabbit anti-human PCSK9 antibody (Cat# ab181142, 1:3000). (d) Serum titration after immunization with hPCSK9. The immune serum (antiserum) from mice immunized with hPCSK9 was titrated in dilutions from 1:200 to 1:640,000 and tested for antigen specificity by ELISA. Native mouse serum (pre-immune serum) was used as a negative control. (e) Screening of positive hybridoma clone secreting mAbs against hPCSK9 by ELISA. Cell culture medium was

used as the negative control (NC). (f) 10% (w/v) SDS-PAGE analysis of the purified m5E12. The purified antibody m5E12 was analyzed under nonreducing condition (lane 1) and reducing condition (lane 2).

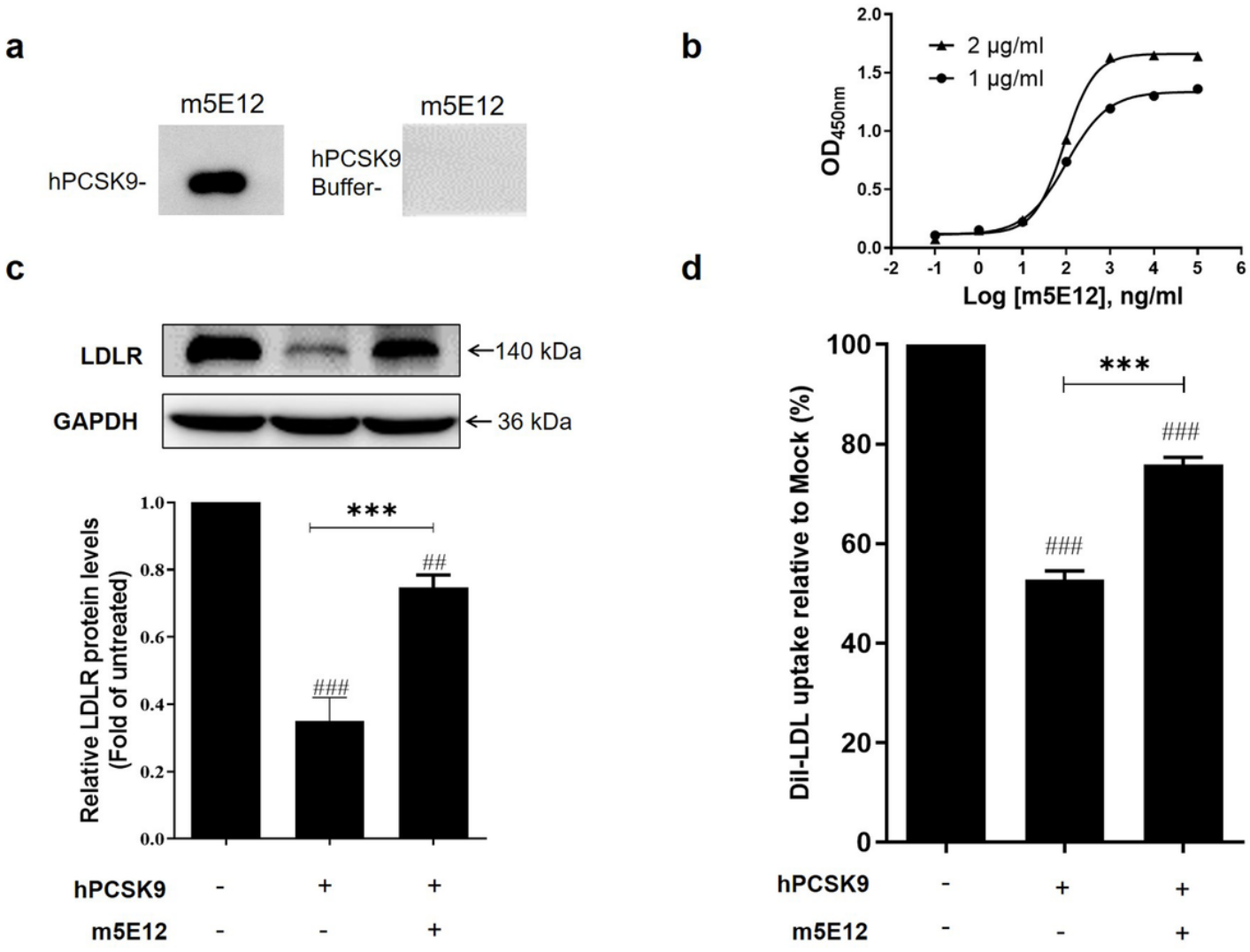

Figure 2

Characterization of mAb 5E12. (a) Western blot analysis revealed that the hPCSK9 protein is specifically recognized by mAb 5E12. The solvent vehicle of hPCSK9 protein (PBS buffer) was served as a negative control. (b) Nonparametric test fitting curve of the results of non-competitive ELISA. The EC50 was equal to 81.36 ng/ml and 90.42 ng/ml when the concentrations of hPCSK9 protein were 1 μg/ml and 2 μg/ml respectively, by which Kaff could be calculated as 1.04×109 M-1, using the formula of Kaff = (n-1)/2(n[Ab']t-[Ab]t). (c) Inhibitory effect of m5E12 on PCSK9-mediated LDLR degradation as assessed by Western blot analysis. HepG2 cells were treated with 20 μg/mL hPCSK9 alone or co-treated with 50 μg/mL m5E12 for 12 h, then the protein levels of LDLR were determined by Western blot. The changes of LDLR were calculated relative to that of the Mock group (vehicle control) after calibration with GAPDH in each lane. (d) Effect of m5E12 on PCSK9-mediated inhibition of LDL-C uptake in HepG2 cells. ## P<0.01 and ### P<0.001 vs. Mock group; ***P<0.001 vs. hPCSK9 group. Data are means ± SEM of 3 independent experiments.

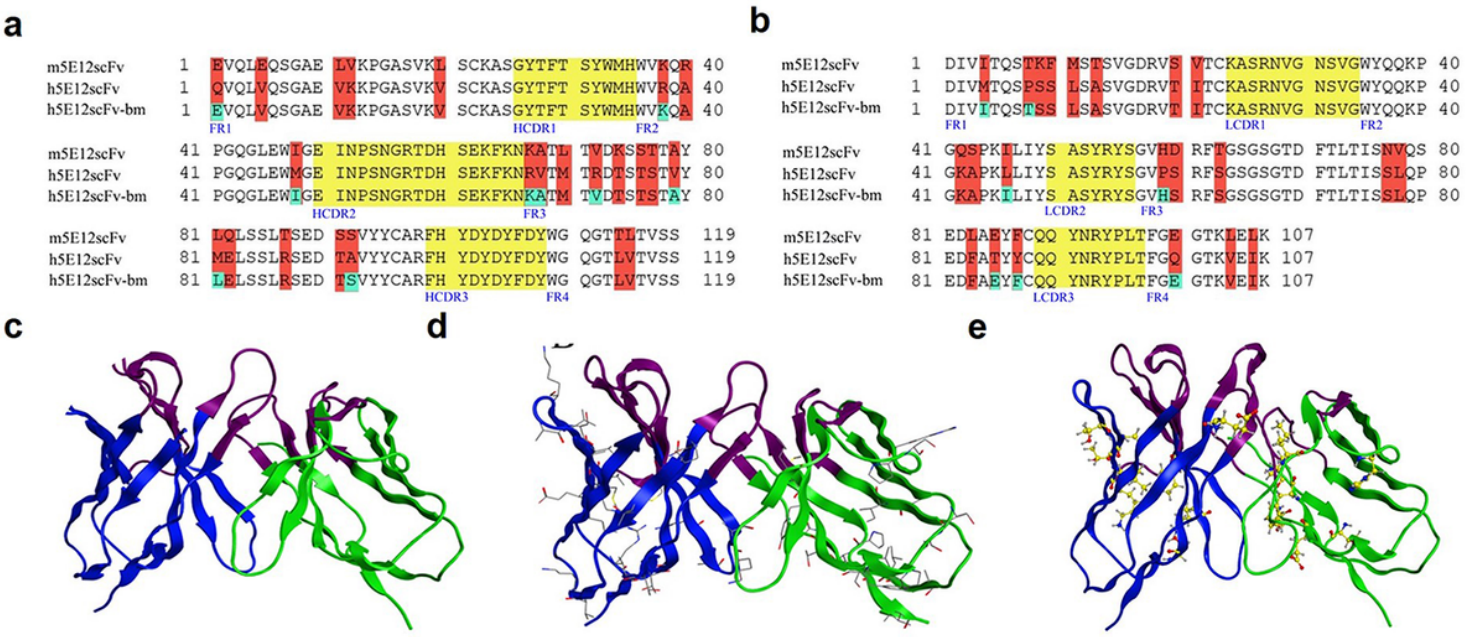

Figure 3

Humanization of m5E12scFv. (a-b) Sequence alignment of the VH (a) and VL (b) domain of m5E12scFv, h5E12scFv and h5E12scFv. The canonical residues back-mutated to murine residues in FRs of h5E12scFv-bm are marked in green, and the residues different between murine and humanized scFvs are marked in red. The CDRs are marked in yellow. (c) The homology modelled structures of m5E12scfv. The murine heavy chain (PDB ID: 10AR_H) and murine light chain (PDB ID: 1H8N_A) were used as templates for modelling of m5E12scFv. (d) The homology modelled structures of h5E12scfv. the homo heavy chain (PDB ID: 3HC0_H) and homo light chain (PDB ID: 1T04_A) were used as templates for modelling h5E12scfv. (E) The homology modelled structures of h5E12scFv-bm. The humanized heavy chain (PDB ID: 1IT9_H) and homo light chain (PDB ID: 1AD9_L) were used as templates for modelling h5E12scFv-bm. The FRs of heavy chains and light chains are presented in blue and green, respectively; the CDRs of variable regions are presented in purple; the residues in h5E12scFv different from m5E12scFv are presented in the skeletal formula; the back-mutated residues in h5E12scFv-bm are presented in the ball-and-stick formula.

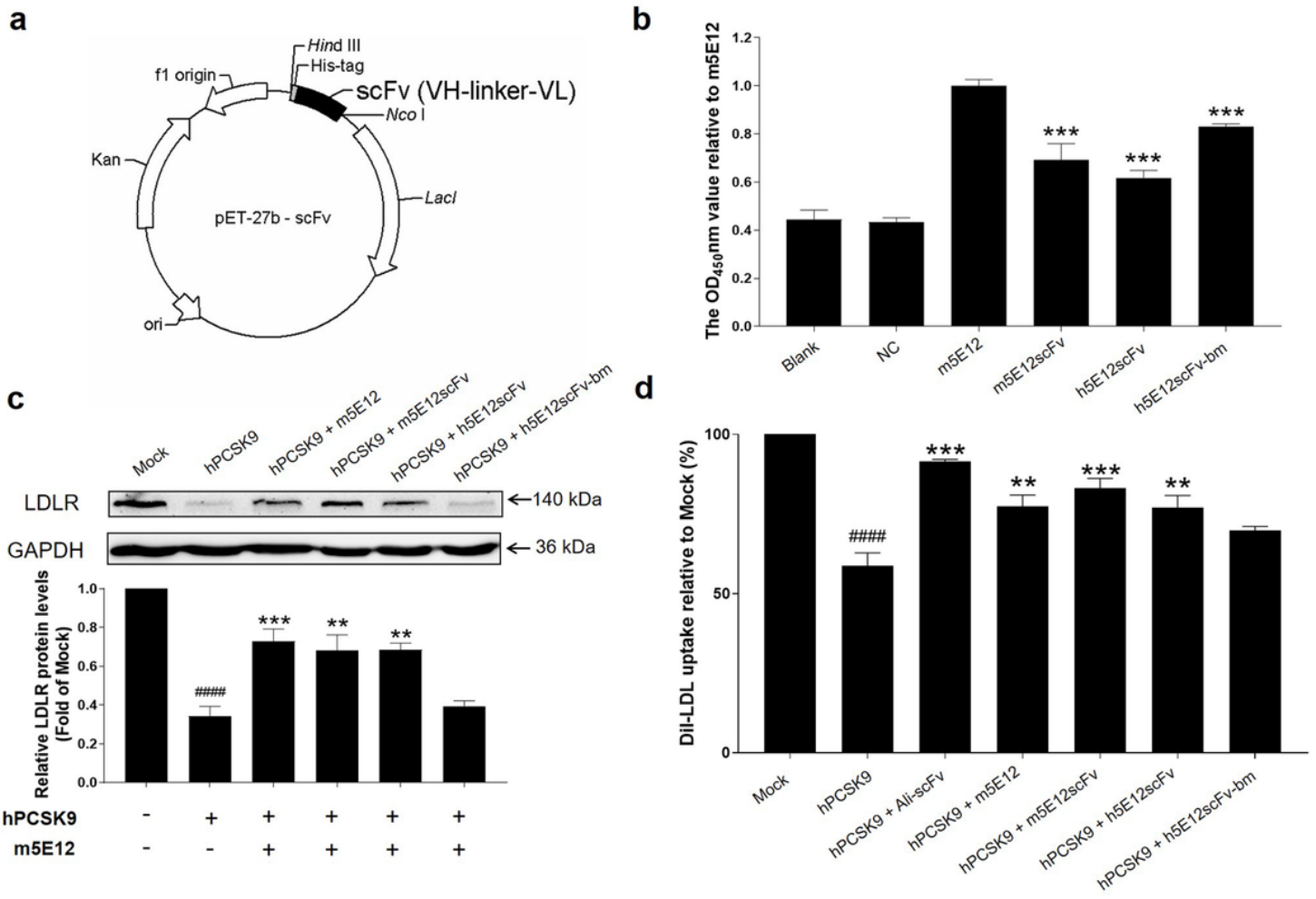

Figure 4

Selection of humanized 5E12 scFv. (a) Schematic representation of plasmids expressing anti-hPCSK9 scFv. The restriction sites (Nco I/Hind III) used for the construction of the vector are indicated. (b) Competitive ELISA for determining binding specificity of scFvs in comparison with parental antibody m5E12. hPCSK9-coated microplates were incubated with 0.5 μg/ml m5E12 mixed with or without 300 μg/ml scFvs (m5E12scFv, h5E12scFv or h5E12scFv-bm) at 37°C for 2h. An equal volume of the vehicle (3% BSA in PBS) was used as the negative control, and wells without any treatment were taken as blank control. The result suggested that the scFvs could compete against parental antibody m5E12 to bind to hPCSK9, and the binding ability of m5E12scFv and h5E12scFv were stronger than h5E12scFv-bm. NC, negative control. ***P<0.001 vs. m5E12 group. (c) Inhibitory effect of humanized 5E12scFv on PCSK9-mediated LDLR degradation as assessed by Western blot analysis. HepG2 cells were treated with 20 μg/mL PCSK9 alone or co-treated with 50 μg/mL m5E12 for 12 h, then the protein levels of LDLR were determined by Western blot. The changes of LDLR were calculated relative to that of the Mock group (vehicle control) after calibration with GAPDH in each lane. (d) Effect of humanized 5E12 scFv on PCSK9-mediated inhibition of LDL-C uptake in HepG2 cells. ####P<0.0001 vs. Mock group; **P<0.01, ***P<0.001 vs. hPCSK9 group. Data are means ± SEM of 3 independent experiments.

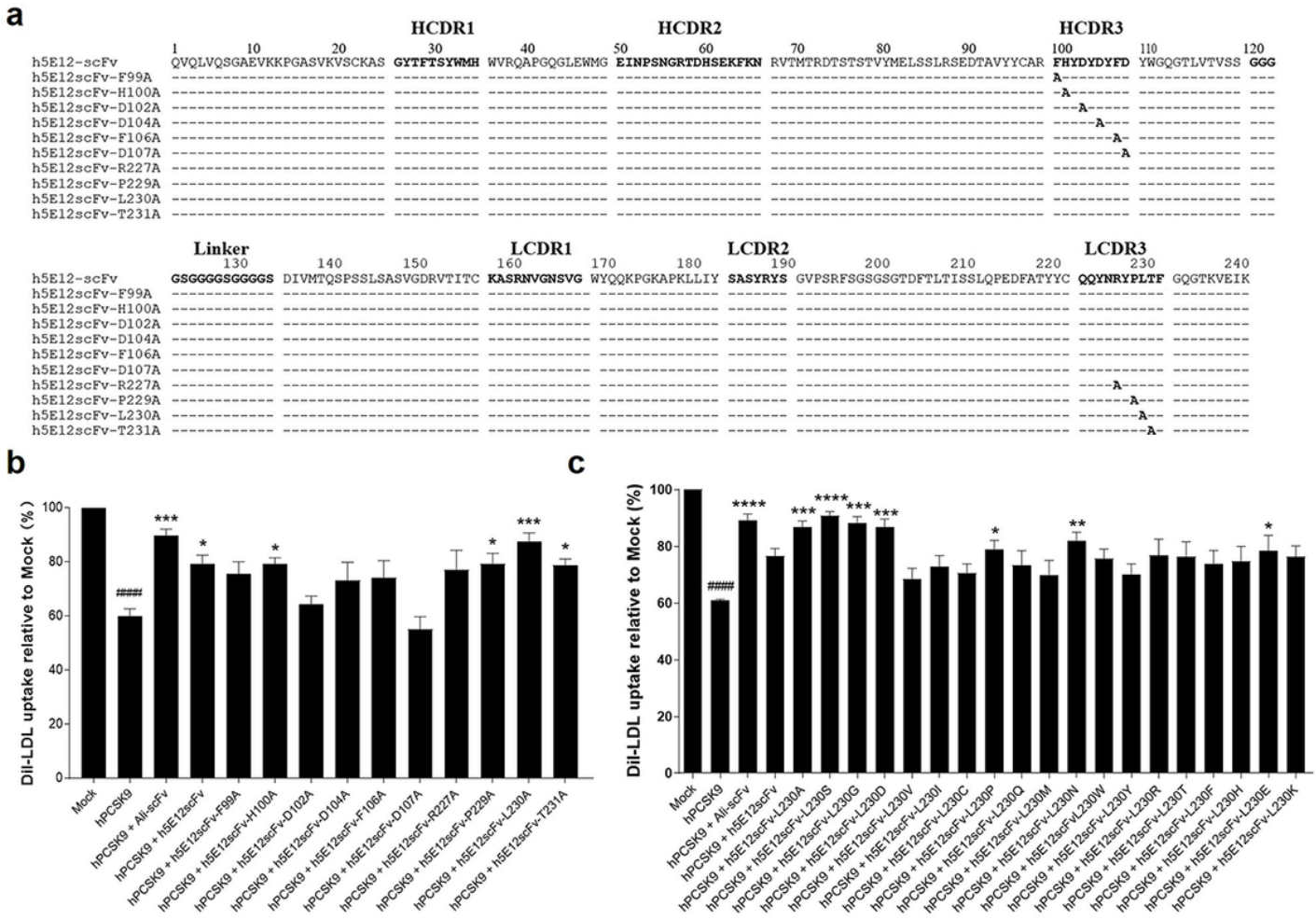

Figure 5

Affinity maturation and selection of h5E12scFv in vitro. (a) Alignment of the amino acid sequences of h5E12scFv with its corresponding alanine-scanning variants. Dashes (-) represent the same residue as h5E12scFv. (b) Effect of the alanine-scanning mutants of h5E12scFv on PCSK9-mediated inhibition of LDL-C uptake in HepG2. The result revealed that L230 was not necessary for maintaining h5E12scFv's activity and its modification might improve the hPCSK9 inhibitory effect of h5E12scFv. (c) Effect of the saturated mutagenesis variants of h5E12scFv on PCSK9-mediated inhibition of LDL-C uptake in HepG2. The result showed that h5E12scFv-L230S was the most potent hPCSK9 inhibitor among all the h5E12scFv variants. ### P<0.001, #### P<0.0001 vs. Mock group; *P<0.05, ** P<0.01, *** P<0.001, **** P<0.0001 vs. hPCSK9 group. Data are means ± SEM of 3 independent experiments.

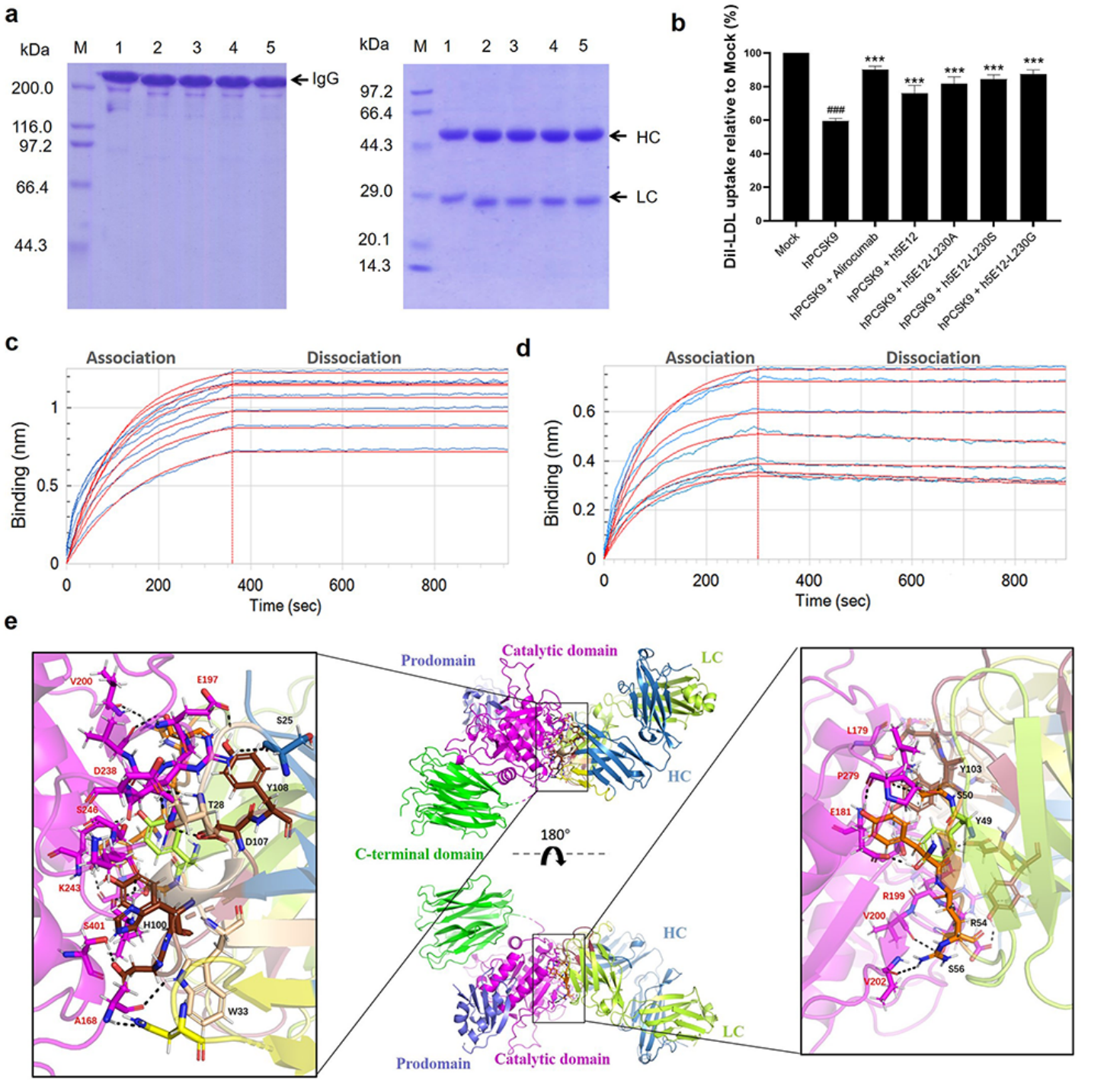

Figure 6

Preparation and identification of the full-length anti-PCSK9 antibodies. (a) SDS-PAGE analysis of purified anti-PCSK9 mAbs under non-reducing (left panel, 10% gel) and reducing (right panel, 12% gel) conditions. M, molecular weight marker; Lane 1, Alirocumab; Lane 2, h5E12; Lane 3, h5E12-L230A; Lane 4, h5E12-L230S; Lane 5, h5E12-L230G. (b) Effect of the anti-PCSK9 mAbs on PCSK9-mediated inhibition of LDL-C uptake in HepG2. ###P<0.001 vs. Mock group; *** P<0.001 vs. hPCSK9 group. Data are means ± SEM of 3 independent experiments. (c-d) Kinetics measurement of h5E12-L230G (c) and Alirocumab (d) binding to surface-immobilized antigen hPCSK9 using a ForteBio Octet QKe system. The biotinylated-hPCSK9 was loaded onto SA sensors and exposed to two-fold serial dilutions of antibody (800, 400, 200, 100, 50, 25, and 12.5 nM) solutions measure the

association rate (kon), and then moved to SD buffer (PBS, pH 7.4, 0.02% Tween 20, 0.1% BSA) without antibodies measure the dissociation rate (koff). Blue and red lines show experimental and calculated fitting sensorgrams, respectively. Kinetic parameters were calculated by global fitting the binding curves (red lines) using Octet data Analysis software 7.1. (e). Intermolecular interaction analyses of the h5E12-L230G with hPCSK9. The prodomain, catalytic domain and C-terminal domain of hPCSK9 were coloured in slate, magenta and green, respectively. The heavy chains' variable regions were shown in skyblue and the light chains' variable regions in limon. h5E12-L230G binds to the catalytic domain of PCSK9. Key residues involved in the interactions were represented as sticks models and labelled in red font for PCSK9' key residues, black for h5E12-L230G' key residues.

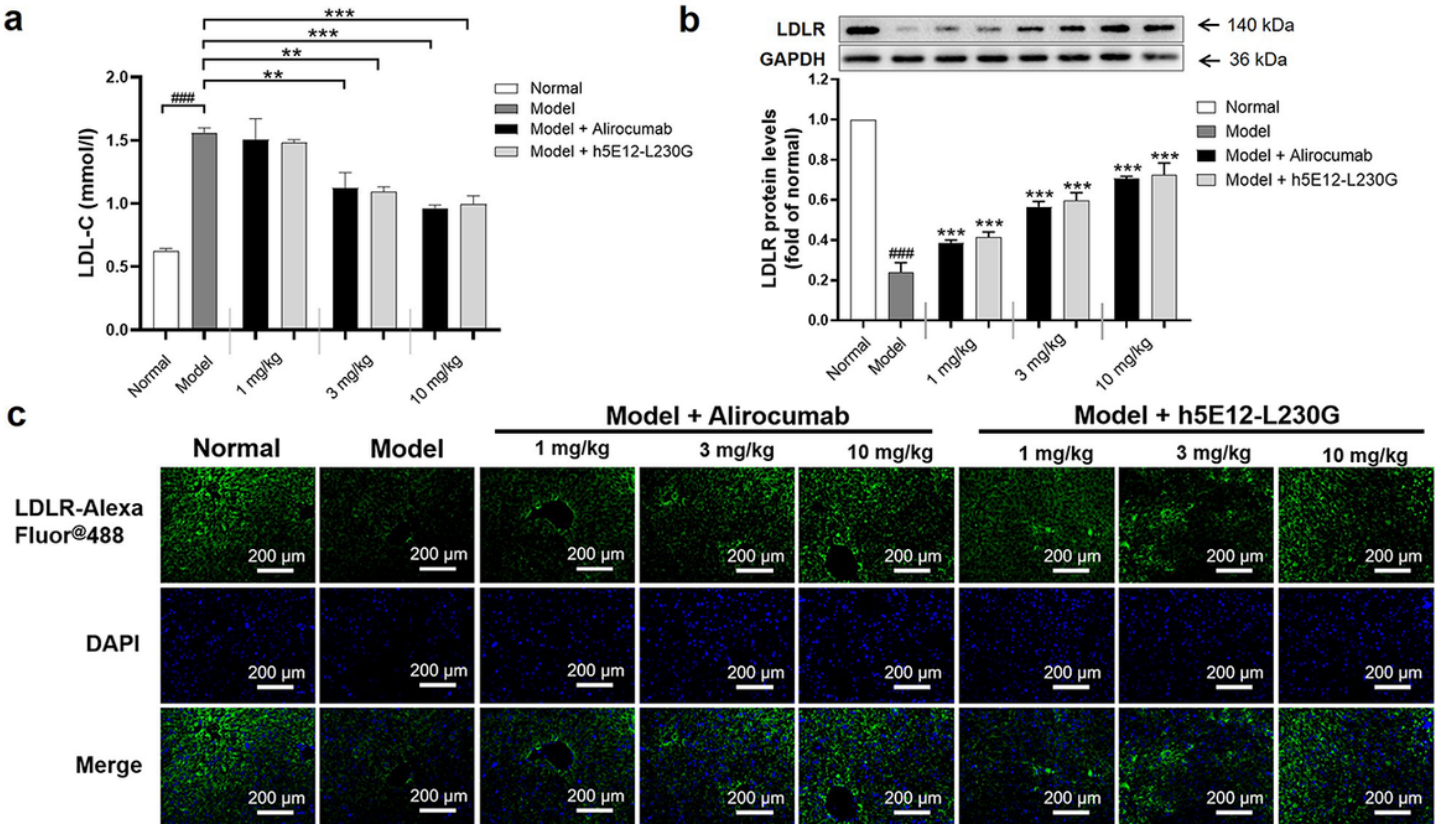

Figure 7

In vivo hypolipidemic efficacy of h5E12-L230G in hypercholesterolemic model mice. (a) h5E12-L230G demonstrated a significant dose-dependently LDL-C lowering effect similar to Alirocumab. Results were expressed as mean ± SEM (n=6 per group). See Table 4 for detailed value. (b-c) Hepatic LDLR changes in h5E12-L230G or Alirocumab treated C57BL/6 mice were detected by Western blot (b) and Immunofluorescence (c). ###P< 0.001 vs. Normal group. **P< 0.01, ***P< 0.001 vs. Model group. Scale bars = 100 μm. Data are representative of 3 independent experiments with similar results.

Supplementary Files

This is a list of supplementary files associated with this preprint. Click to download.

- Supplementarymaterials.doc